Zahn, R., Comas, M.C., and Klaus, A. (Eds.), 1999
Proceedings of the Ocean Drilling Program, Scientific Results, Vol. 161

44. THE ORIGIN AND TECTONIC HISTORY OF THE ALBORAN BASIN: INSIGHTS FROM LEG 161 RESULTS[1]

M.C. Comas,[2] J.P. Platt,[3] J.I. Soto,[2] and A.B. Watts[4]

ABSTRACT

The Ocean Drilling Program (ODP) Leg 161 drilled in the Western Mediterranean Sea (May–June, 1995) to investigate outstanding processes in the origin and structural evolution of the Alboran Basin. Studies at the Site 976 basement high, in the West Alboran Basin, demonstrate that the basin is floored with metamorphic rocks of continental origin (high-grade schist, migmatitic gneiss, marble, and calc-silicate rock, cross-cut by granite dikes) from the Alpujárride Complex of the Alboran Crustal Domain. Sediments encountered at the tops of the basement high are middle Miocene in age (about 11–12 Ma, late Serravallian). The pressure-temperature (P-T) evolution of the high-grade schist shows heating during decompression, from pressures of up to 10.5 kbar at about 500°C (corresponding to a burial depth of around 40 km) to final temperature conditions of 650º–700°C at a pressure of 3–4 kbar. The decompression was followed by cooling to T < 500º–600°C and P < 2–3 kbar. Ar/Ar dating on coexisting muscovite and biotite shows that this cooling occurred from 426°C at 20.0 ± 0.2 Ma to 330°C at 19.2 ± 0.7 Ma. Apatite fission-track shows that final cooling of the basement below 60°C took place at 18.3 ± 1.0 Ma (Burdigalian). Site 976 reveals two periods of subsidence, in the middle Miocene (synrift subsidence, at 11–10.7 Ma; rate of 3 km/m.y.) and since the latest Pliocene (postrift transtensive? subsidence, at 2.5–0 Ma earliest rate of 0.5 km /m.y.), and uplift at 5–2.5 Ma (early Pliocene). Conspicuous lateral variations in rift-related subsidence phases in the basin suggest migration of the locus of extension, and probably also changes in tectonic-transport direction during the Miocene rifting. Miocene crustal thinning in the Alboran Domain is related to low-angle intracrustal detachments and shallow normal faulting. Since the latest Tortonian, relatively uplifted and subsided areas coexist, but a generalized, continuous, and slower subsidence developed within the marine basin. Drilling results in the East and South Alboran basins (Sites 977, 978, and 979) define the timing of the later (post-Messinian) tectonic reorganization of the Alboran Basin into the present-day Alboran Sea basin. Ar/Ar dating of reworked but representative volcanic pebbles from tholeiitic, calc-alkaline, and shoshonitic series (Sites 977 and 978) constrains episodes of middle-to-late Miocene volcanism in the eastern Alboran region at 12.1 ± 0.2 Ma, 9.90 ± 0.4 Ma, 9.29 ± 0.02 Ma, and 6.1 ± 0.3 Ma. Incompatible elements in these rocks include both depleted (MORB-source) component and an ocean-island or plume-type component ("arc signature"). Calc-alkaline magmatic affinities and incompatible-element systematics were considered to support a Miocene oceanic subduction zone (from 6 Ma to at least 12 Ma) beneath the eastern Alboran region. However, these magmatic signatures prove to have also originated from variable crustal-contamination of MORB-type melts, produced by shallow melting during asthenosphere-mantle upwelling. Alternatively, modeled P-T paths in basement rocks suggest removal of mantle lithosphere below about 60 km depth (to explain further heating during decompression at shallow depth) and rapid exhumation during lithosphere stretching (4.5 km/m.y.), followed by final cooling with a minimum exhumation rate of 4 km/m.y. It took ~9 m.y. for the exhumation of the basement rocks from 40 km depth to reach the surface at about 18 Ma, thus suggesting that extension in the Alboran Domain started at about 27 m.y. (late Oligocene), before the marine transgression occurred. We consider that strong evidence from rocks at the Site 976 basement high favors models that use the removal of mantle lithosphere as the driving force for extension generating the Alboran Basin. Further geological and geophysical data from the westernmost Mediterranean region are needed to corroborate our conclusions to define a fully satisfying model for the Neogene evolution of the lithosphere beneath the Alboran Basin.

INTRODUCTION

The unique position of the Mediterranean Sea within an area where two continents display the progressive effects of Tertiary-to-Holocene convergence makes this region a relevant locus for studying lithosphere behavior in continental collisional settings. Lithosphere deformation in certain areas of the Mediterranean may be, to some extent, independent of the motions of the major plates bounding the region; hence, analysis of the mechanisms causing this deformation can improve our general understanding of geodynamic processes. Current awareness of Mediterranean geology indicates that some late Tertiary basins in the western Mediterranean, often described as Mediterranean "back-arc basins" (Horvath and Berckhemer, 1982), were formed by late-orogenic extension on the sites of former orogens. These former orogens were constructed as a result of the Cretaceous-to-Paleogene collision of the Eurasian and African plates. Much of the current debate and controversial hypotheses on the genesis of these basins center on the processes that caused the Alboran Sea basin and its link with the tectonic evolution of the Betic-Rif orogen (Fig. 1). The Alboran Basin apparently initiated on thickened continental crust and developed by lithosphere stretching behind an arcuate thrust belt; sediments accumulated on thinned continental crust, and magmatic activity, ranging from calc-alkaline to alkaline, accompanied the basinal evolution. The onset of crustal thinning appears to have closely followed continental collision, and thrusting in the surrounding Betic and Rifean mountain belt was active coevally with extension in the basin.

The Ocean Drilling Program (ODP) Leg 161 (Comas, Zahn, Klaus, et al., 1996) was planned to drill a transect of six sites (Sites 974 to 979) in the Western Mediterranean, from the Tyrrhenian Basin to immediately east of the Strait of Gibraltar in the Alboran Basin. Holes in the Tyrrhenian Sea and on the Menorca Rise were dedicated exclusively to paleoceanographic objectives, but the four sites drilled in the Alboran Sea were aimed at testing geodynamic models dealing

[1]Zahn, R., Comas, M.C., and Klaus, A. (Eds.), 1999. *Proc. ODP, Sci. Results,* 161: College Station, TX (Ocean Drilling Program).

[2]Instituto Andaluz de Ciencias de la Tierra, CSIC and University of Granada, Campus, Fuentenueva, 18002 Granada, Spain. Comas: mcomas@goliat.ugr.es

[3]Department of Geological Sciences, University College London, Gower Street, London WC1E 6BT, United Kingdom.

[4]Department of Earth Sciences, University of Oxford, Parks Road, Oxford OX1 3PR, United Kingdom.

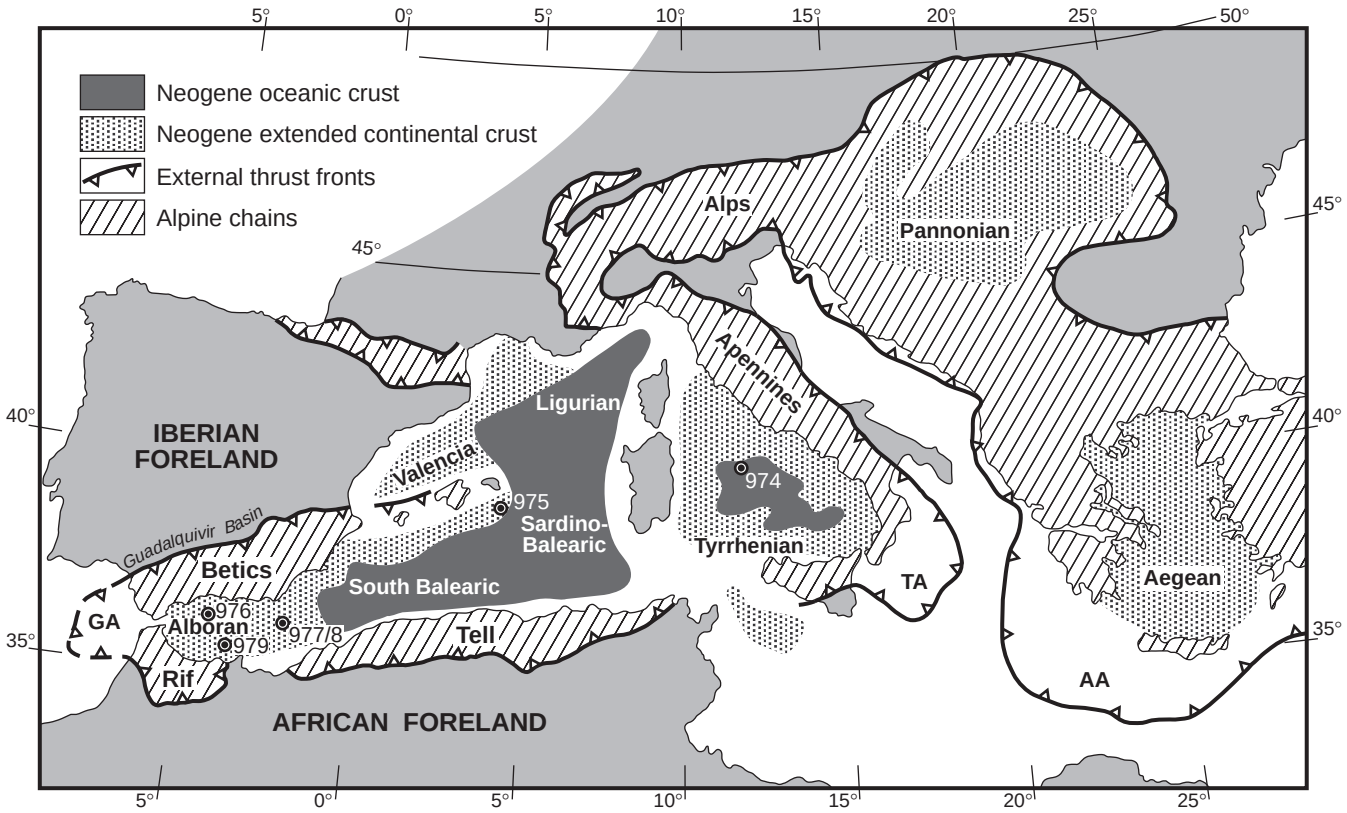

Figure 1. Location of ODP Leg 161 sites in a tectonic sketch of the Mediterranean Sea, showing Neogene extensional basins and external front of surrounding Alpine thrust belts. AA = Aegean Arc, GA = Gibraltar Arc, TA = Tyrrhenian Arc.

with the formation and tectonic behavior of the Alboran Basin (Figs. 2, 3).

The goal of this paper is to synthesize the data and interpretations pertaining to the basement rocks and the structure of the Alboran Basin. We integrate the results of drilling with regional geological and geophysical data and interpret the deep and shallow seismic-reflection profiles to construct structural maps and geological sections of the region. The conclusions drawn from all these data constrain the nature and structure of the crust beneath the Alboran Sea, and the origin and tectonic history of the basin.

The main data and specific scientific results discussed here proceed either from manuscripts accepted for the Leg 161 *Proceedings of the Ocean Drilling Program, Scientific Results* or from papers sent to the outside literature. Petrographic, geochemical, microstructural, and thermobarometric analyses (López Sánchez-Vizcaíno and Soto, Chap. 18, this volume; Prosser et al., Chap. 20, this volume; Soto and Platt, in press; Soto et al., Chap. 19, this volume; Spadea and Prosser, Chap. 28, this volume) determine the lithologies, sedimentary protoliths, fabrics, and stages of evolution in terms of P-T paths (pressure-temperature variations) of cored metamorphic rocks from the basement (Platt et al., 1996). The study of breccia types and fault gouges within the uppermost basement section and at the sediment-basement interface (Comas and Soto, Chap. 25, this volume) ascertain features of brittle deformation. Analyses of processed FMS (Formation MicroScanner) and BHTV (Borehole TeleViewer) images of hole walls (de Larouzière et al., Chap. 24, this volume) investigate the stress field and basement structural pattern. Ar/Ar dating of micas (Platt and Kelley, Chap. 22, this volume) and apatite fission-track analysis (Hurford et al., Chap. 21, this volume) of basement samples yield constraints on the timing of distinct thermal and structural events. Thermal modeling of the P-T-t (Pressure-Temperature-time) paths in basement rocks allows precise geodynamic models to be constrained (Platt et al., in press). Geochemical analysis and Ar/Ar dating of volcanic-rock pebbles from sedimentary gravel-intervals (Hoernle et al., Chap. 27, this volume) provide information on the ages and magmatic affinity of the volcanism from surrounding regions. Studies on the *JOIDES Resolution* seismic survey (Klaus and Shipboard Scientific Party, 1996), combined with the interpretation of multichannel seismic (MCS) profiles around drill sites (Alvarez-Marrón, Chap. 26, this volume; Comas and Soto, Chap. 25, this volume; Tandon et al., 1998), describe the synsedimentary structural history of the basin. Backstripping from Hole 976B and two commercial wells documents some episodes of the subsidence-uplift history of the basin (Rodríguez-Fernández et al., Chap. 5, this volume). Correlations between cored samples and similar rock-units cropping out in the Betic Cordillera have been performed for both the basement (Sánchez-Gómez et al., Chap. 23, this volume) and the sedimentary cover (Rodríguez-Fernández et al., Chap. 5, this volume).

SCIENTIFIC BACKGROUND

Geologic Setting: The Betic and Rif Chains

The Betic (Southern Spain) and Rif (Morocco) Chains, connected through the Gibraltar Strait are elongated east-northeast–west-southwest and northwest-southeast, respectively. The Alboran Sea, in continuity to the east with the South Balearic Basin, is located in the inner part of this arcuate belt. The region as a whole is bounded to the north and south by the Iberian and African forelands, to the west by the Atlantic Ocean, and to the east it is connected to the oceanic Sardino-Balearic Basin (Fig. 1).

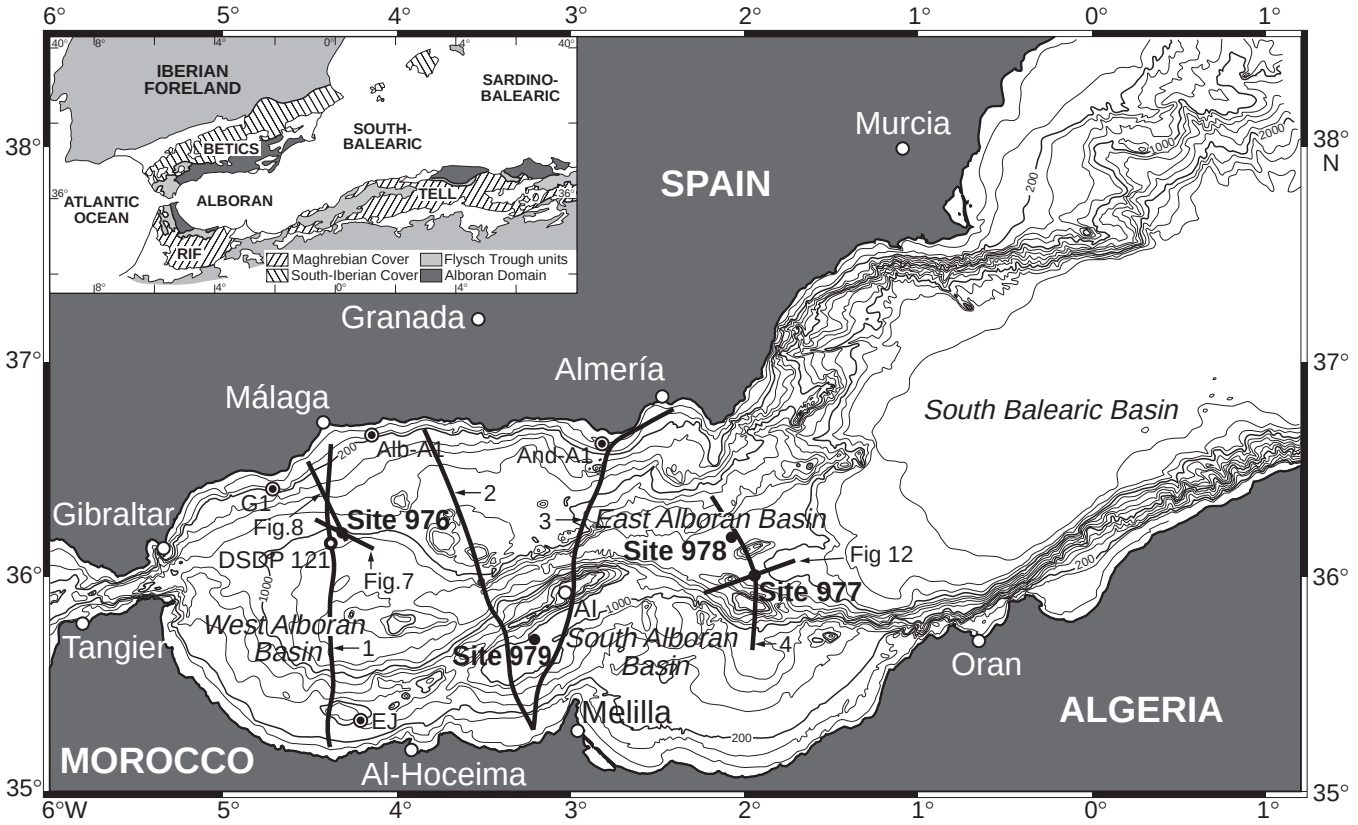

Figure 2. Bathymetry of the westernmost Mediterranean (Alboran and South Balearic seas), showing location of ODP Leg 161 sites, DSDP Site 121, and commercial boreholes offshore. Bathymetry contours in meters, contour interval 200 m. Locations of seismic profiles shown in Figures 7, 8, and 12, and position of *Conrad* lines in the back-pocket foldout are marked. *Conrad* MCS reflection profiles: 1 = Lines 827, 2 = Line 825, 3 = Line 824, 4 = Line 823. Inset map: location of the Alboran Sea between the Betic and Rif Chains, main crustal domains are shown. AI = Alboran island. Commercial wells: G1 = Andalucía G1, Alb-A1 = Alboran A1, And-A1 = Andalucía A1, and EJ = El-Jebha.

The peculiarities of these westernmost Mediterranean chains result from their position between two large convergent plates—Africa and Europe—that have had variable directions of relative motion since the late Cretaceous. Kinematic models show that this segment of the plate boundary experienced ~200 km of roughly north-south convergence between the mid-Oligocene and late Miocene, followed by about 50 km of northwest-southeast convergence from the latest Tortonian (9–8 Ma) to the present-day (Dewey et al., 1989; Srivastava et al., 1990; Mazzoli and Helman, 1994; Morel and Meghraoui, 1996).

The complexes and large paleogeographic terrains traditionally recognized in the Betic and Rif Chains belong to four pre-Neogene crustal domains (Fig. 2, inset map): (1) the South-Iberian and Maghrebian passive continental paleomargins (External Zones of the Betic and Rif Chains, respectively), formed of Mesozoic and Tertiary sedimentary rocks; (2) the Flysch Trough Units, remarkably represented in the Rif and Tell regions, comprising nappes of early Cretaceous–early Miocene sediments, that originally occupied a trough over oceanic or very thin continental crust; and (3) the Alboran Crustal Domain (Paleozoic and Mesozoic rocks of the Betic-Rifean Internal Zones), composed mainly of a pre-Miocene metamorphosed thrust-stack that includes three nappe complexes: the Nevado Filábride, Alpujárride, and Maláguide. The mountain ranges in the Betic-Rifean Internal Zones are separated by Neogene intramontane basins (the so-called "Neogene Basins").

The highest complex (the Maláguide) shows only very low-grade metamorphism, whereas the Alpujarride and the underlying Nevado-Filábride Complex show Alpine metamorphic evolution from early high-pressure/low-temperature conditions to later lower-pressure conditions at moderate to locally high temperatures. The high-P/low-T mineral assemblages occurring in these two complexes result from crustal stacking in the Betics and Rif as a result of pre-Miocene (Cretaceous-to-Paleogene) convergence, subduction, and continental collision (Bakker et al., 1989; Goffé et al., 1989; De Jong, 1991; Tubía and Gil Ibarguchi, 1991). The later low-P/high-T metamorphism in parts of the Alpujárride Complex appears to be related with later extension and exhumation of deep crustal rocks (Monié et al., 1994; García-Casco and Torres-Roldán, 1996; Balanyá et al., 1997; Azañón et al., 1997, 1998). The original contractional structures in the orogen have been strongly modified by later extension, and the original boundaries between the main nappe complexes are now generally thought to have been cut or reactivated by large-scale low-angle extensional detachment faults (Platt, 1986; García-Dueñas et al., 1988; Platt and Vissers, 1989; Galindo-Zaldívar et al., 1989; Aldaya et al., 1991; García-Dueñas et al., 1992; Jabaloy et al., 1993; Lonergan and Platt, 1995; among many others).

Structural data show that in the late Oligocene the Alboran Crustal Domain (the original metamorphosed orogenic nappe-stack) thrust outward onto the South-Iberian and Maghrebian continental margins, and the dominant westward propagation of thrusting from the latest Oligocene and early Miocene led to the progression of an arcuate peripheral thrust belt (the Gibraltar Arc). Thrust directions vary from northwest in the Betic Cordillera (Banks and Warburton, 1991; Lonergan et al., 1994) to west in the Gibraltar region (Balanyá and García-Dueñas, 1987, 1988; Platt et al., 1995; Kirker and Platt, 1998) and to west-southwest and south in the Rif (Frizon de Lamotte, 1987;

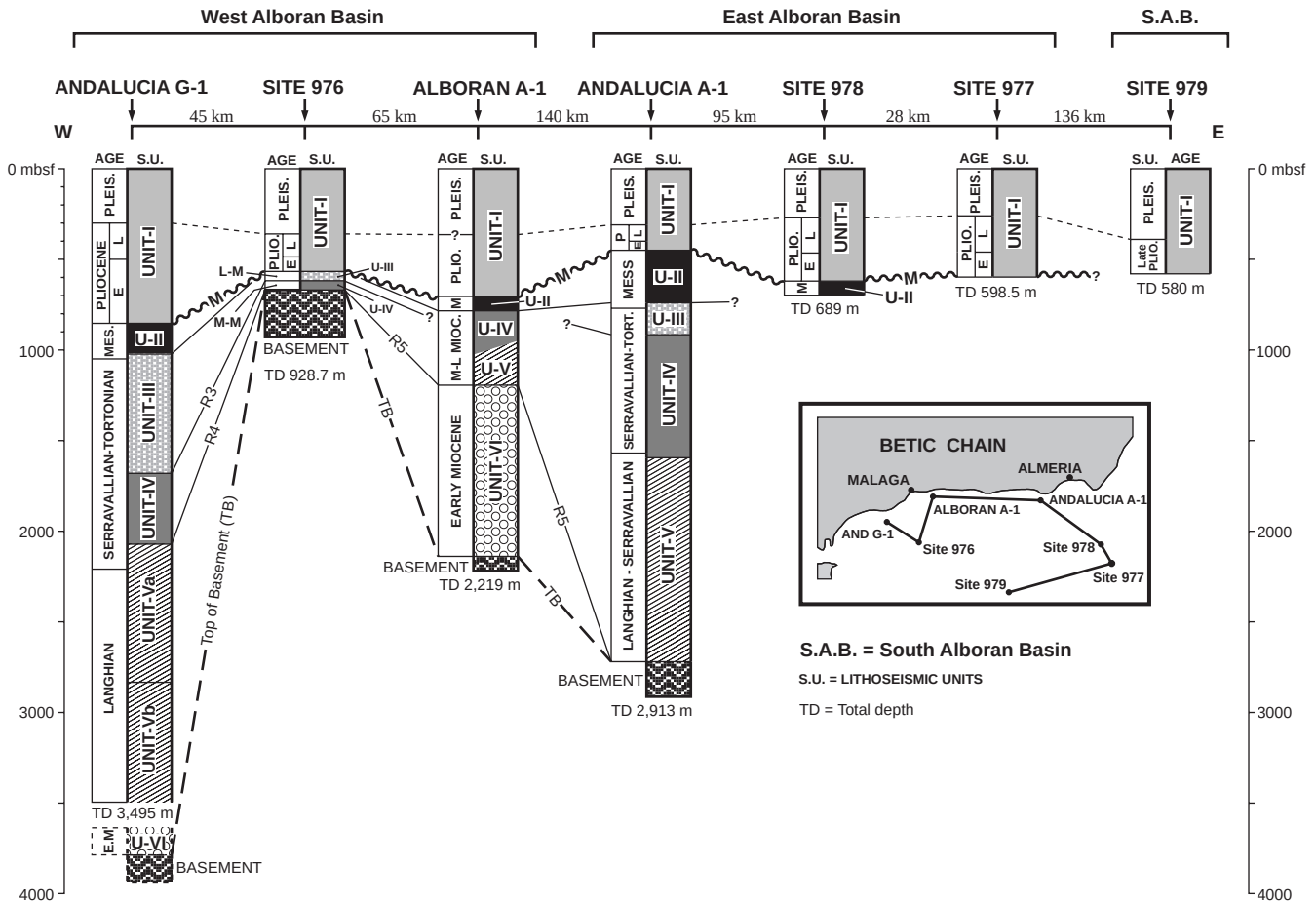

Figure 3. Correlation between sedimentary sequences sampled at Sites 976, 977, 978, and 979 and in commercial wells on the Iberian shelf. Shown are ages, seismic units, major regional reflectors, and drilled metamorphic basement. Correlation is based on MCS analysis, logging, and stratigraphic data. Seismic units and R-reflectors according to Comas et al. (1992). R-reflectors correspond to major unconformities within sediments. M = Messinian unconformity. Ages of Pliocene–Pleistocene sequences from Comas, Zahn, Klaus, et al. (1996). Inset map shows location of commercial boreholes, connecting lines between holes refer to relative position and distances in kilometers shown at the heading of this figure.

Morley, 1992; Platzman et al., 1993). It should be noted that thrusting and shortening in the peripheral belt (the External Zones of the Betic and Rif Chains) were contemporaneous with extension and crustal thinning within the arc, in the Alboran Domain itself. Progression of the arcuate mountain front and extension in its inner part continued during the late Burdigalian and middle Miocene. Recent structural analyses of kinematic vectors in the Alboran Domain cropping out in the Betics have shown two major extensional systems of Miocene age, which have different transport directions: one with a dominant north-northwestward transport sense (the Contraviesa extensional system) during the late Burdigalian–Langhian, and another with a dominant west-southwestward transport sense (the Filabres extensional system) during the Serravallian (García-Dueñas et al., 1988, 1992; Crespo-Blanc et al., 1994; Azañón et al., 1997, 1998; Martínez-Martínez and Azañón, 1997; Martínez-Martínez et al., 1997, in press; among others).

The extensional phase was locally accompanied by a distinctive low-P/high-T metamorphic event and was followed by cooling under low-P conditions. Radiometric age determinations on metamorphic rocks from diverse Alpujárride units reveal that cooling occurred rapidly during the early Miocene at between 22 and 18 Ma (Ar/Ar, K/Ar, and Rb/Sr dating; Zeck et al., 1989, 1992; Monié et al, 1994). Fission-track data in these rocks indicate that cooling continued until 18 to 16 Ma (Andriessen and Zeck, 1996; Sosson et al., 1998). Geochronologic data from volcanic or subvolcanic rocks cropping out in the Betic and Rif Chains prove that tholeiitic to calc-alkaline magmatism has accompanied the extensional processes (Torres-Roldán et al., 1986; Zeck et al., 1989, 1992; Monié et al., 1994; Bellon et al., 1983; Di Battistini et al., 1987; Hernandez and Bellon, 1985; Hernandez et al, 1987).

Shortening in the peripheral belt and general crustal stretching and extension in the Alboran Domain appear to have concluded by the late Miocene. Since the late Tortonian, a compressional regime, producing folding, reverse faulting, structural inversions of previous normal faults, and strike-slip faults, accounted for a general contractive structural reorganization of the Betic and Rif Chains (Weijermars, 1985; Aït Brahim and Chotin, 1989; Morel, 1989; Montenat et al., 1992; Galindo-Zaldívar et al., 1993; Meghraoui et al., 1996; Martínez-Martínez et al., 1997). Contemporaneous volcanism, made up mainly of shoshonitic to lamproitic lavas and alkaline basalts, erupted extensively in the eastern sectors of the Betic and Rif Chains (Bellon et al., 1983; Di Battistini et al., 1987; Hernández and Bellon, 1985; Hernandez et al., 1987). Regional data indicate that compression was northwest-southeast during the late Tortonian, rotating to north-south from the late Tortonian to the middle Pliocene, and changing to a north-northwest–south-southeast during the rest of the Pliocene and Pleistocene (Ott d'Estevou and Montenat, 1985; Montenat et al., 1987; De Larouzière et al., 1988). Late Tortonian east-west–trending folds and latest Miocene to Holocene wrench tectonics (north-south, and west-northwest–east-south strike-slip fault systems) produced shortening of the whole region (the Betic and Rif Chains and the marine realm), with concomitant uplifting and pro-

gressive emersion at the marine-basin margins. Thus, from the late Tortonian onward, some peripheral marine depocenters (extensional grabens) of the ancestor (early and middle Miocene) Alboran Basin progressively emerged, resulting in continental basins during the Pliocene. Neogene marine sequences similar to those filling the basin beneath the Alboran Sea (see below) are widespread in several intramontane depressions and corridors of the emerged regions (the Betic and Rifean onshore "Neogene Basins"; Aït Brahim and Chotin, 1989; Montenat et al., 1987; Sanz de Galdeano and Vera, 1992), proving an original greater north-south extent of the Alboran Basin beyond the present limits of the sea.

The Alboran Basin

The Alboran Sea is about 400 km by 200 km, exhibiting a complex seafloor morphology with several sub-basins, ridges, and seamounts, reaching a maximum depth of 2 km. The Alboran Ridge (180 km in length), the most prominent northeast-southwest linear relief across the Alboran Sea, emerges locally to form the small, volcanic Alboran Island. From the present seafloor morphology, three main sub-basins, named the West, East, and South Alboran Basins, have traditionally been distinguished (Fig. 2).

Multichannel seismic reflection (MCS) profiles evidence that the major sedimentary accumulation (up to 8 km thick) is located in the West Alboran Basin (Fig. 4). Seismic facies from the sedimentary cover have been described in numerous papers, and commercial wells (Figs. 2–4) provide information on sediment types and ages (early Miocene to Pleistocene) beneath the margins of the West Alboran Basin (Comas et al., 1992; Watts et al., 1993; Chalouan et al., 1997; and references therein). Nevertheless, there are no samples from the lowermost sediments in the major depocenter in the West Alboran Basin (Fig. 4; see Fig. 16 on back-pocket foldout, this vol-

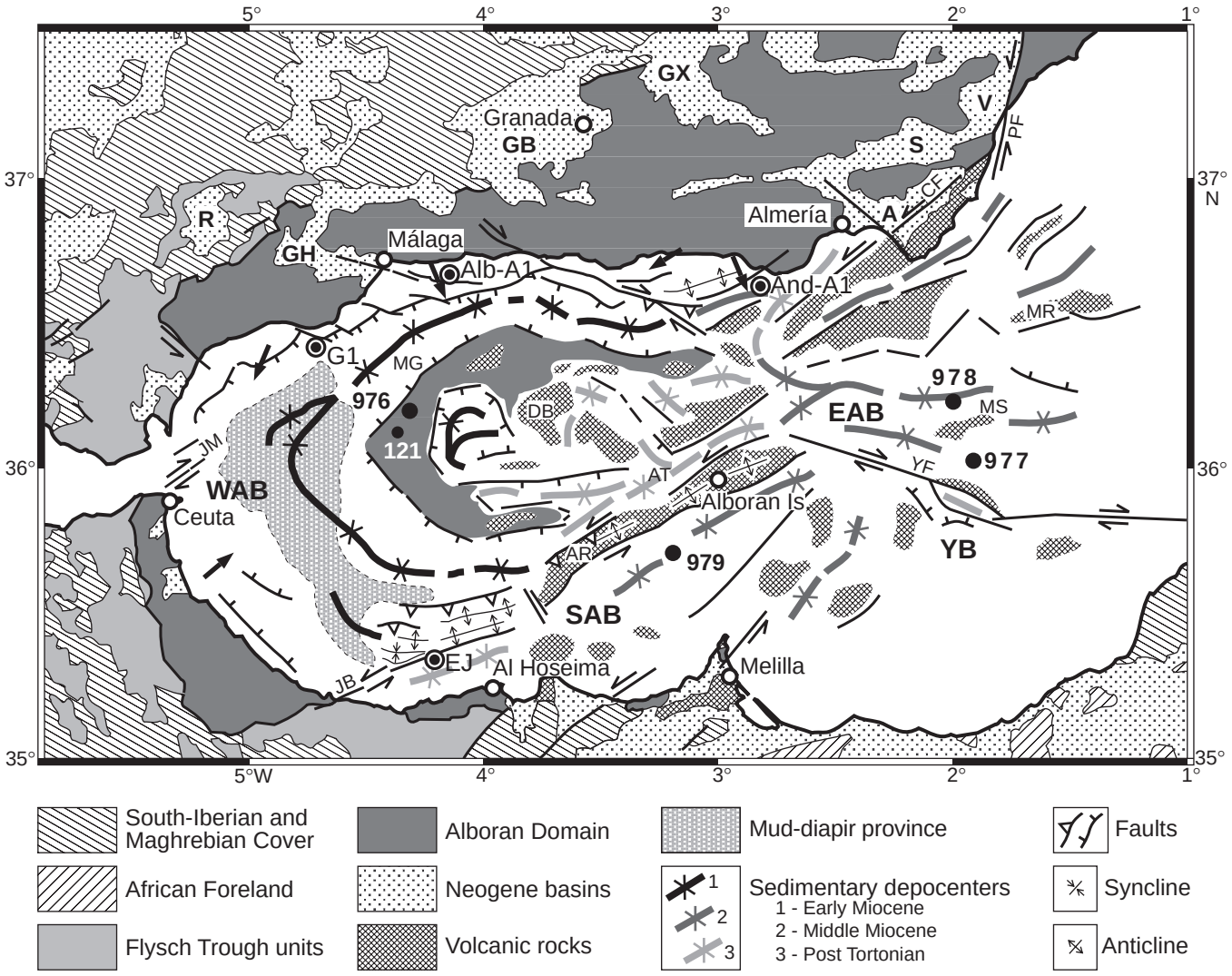

Figure 4. Structural map of the Alboran Basin and surrounding areas showing early Miocene to Holocene structures and main sedimentary depocenters (based on MCS, commercial well data, and Leg 161 results). Measurable directions of middle Miocene extension are indicated by black arrows. Positions of DSDP 121 and ODP Leg 161 sites are shown. Note the onshore Neogene Basins (including Miocene and/or Pliocene marine sediments) cropping out in Spain or Morocco. Main sedimentary depocenters in the Alboran Sea are shown: 1 = Depocenters comprising lower Miocene to Pleistocene deposits; 2 = Depocenters consisting of middle Miocene to Pleistocene deposits; 3 = Depocenters comprising Messinian/Pliocene to Pleistocene deposits. A = Almeria Basin; AR = Alboran Ridge; AT = Alboran Trough; CF = Carboneras Fault; DB = Djibouti bank; EAB = East Alboran Basin; GB = Granada Basin; GH = Guadalhorce Basin; GX = Guadix Basin; JB = Jebha Fault; JM = Jehbel-Mussa Fault; MG = Málaga Graben; MR = Maimonides ridge; MS = Al-Mansour Seamount; PF = Palomares Fault; R = Ronda Basin; S = Sorbas Basin; SAB = South Alboran Basin; V = Vera Basin; YB = Yusuf Basin; YF = Yussuf Fault; WAB = West Alboran Basin. Commercial wells as in Figure 2.

ume). In the South and East Alboran basins, and at the transition to the South Balearic Basin, sediments are probably <4 km thick and lower sediments in major depocenters may be as old as middle Miocene, as suggested by seismic correlations with the El-Jebha and Andalucía-A1 wells. Nonetheless, samples of the lowermost sedimentary sequences in the East and South Alboran basins do not exist either. Before Leg 161, sediment samples from the deep-marine realm existed only from DSDP Site 121 (Ryan, Hsü et al., 1973; Fig. 2).

A straightforward correlation appears with the seismic stratigraphy described in the northern (Comas et al., 1992; Jurado and Comas, 1992) and southeastern (Chalouan et al., 1997) margins of the Alboran Basin. Six seismic stratigraphic units (labeled VI-I from base to top, Fig. 3), tied to the commercial wells off the coast of Spain, have been recognized within the seismic record of the basin (Jurado and Comas, 1992). According to these data (Fig. 3), the older marine deposits overlying the basement beneath the Spanish margin are latest Aquitanian?–Burdigalian in age, and consist of olistostromes containing clastic material and under-compacted shales (seismic Unit VI). Middle to lower-upper Miocene deposits, seismic Units V (Langhian) and IV (Serravallian/early Tortonian) consist of under-compacted shales at the base, passing upward into graded sand-silt-clay turbidite. Sediments from seismic Unit III (late Tortonian) are formed of sandstone intervals that alternate with claystone and silty-clay beds, also corresponding to turbidite layers. Volcaniclastic levels intercalate throughout the middle and upper Miocene sequences. The Messinian deposits (seismic Unit II) consist of marine siliciclastic or shallow carbonate facies, with occasional gypsum and anhydrite intervals. Messinian Unit II has a nearly uniform maximum thickness of about 250 m (about 200 ms TWT) across the entire Alboran Sea basin; furthermore, there exist wide areas in the basin lacking in Messinian sediments, probably due either to erosion or no deposition. A well-developed Messinian-evaporite (thick salt) sequence is absent, in contrast with the neighboring Mediterranean basins to the east (Ryan; Hsü et al., 1973). The Pliocene to Pleistocene sediments (seismic Unit I) sampled in commercial wells consist mainly of fine-grained distal marls, clays, and scarce interbedded sandstones. The extensive diapir province in the West Alboran Basin (Fig. 4) involves sediments from Units VI and V and likely comprises under-compacted, over-pressured material from these units (Comas et al., 1992; Pérez-Belzuz et al.,1997).

In the central region of the Alboran Sea (outside the main subbasins), most sediments above the acoustic, probably volcanic, basement are post-Miocene in age (Fig. 4; e.g., Maldonado et al., 1992; Comas et al., 1992; Watts et al., 1993; Soto et al., 1996; Comas et al., 1997).

Major basin-wide correlatable angular unconformities (Fig. 3) within the sedimentary cover occur at the top of the Burdigalian sediments (top of seismic Unit VI, reflector R5), within Tortonian sediments (base of seismic Unit III, reflector R3), and at the base of the Pliocene–Pleistocene sequence (base of seismic Unit I, reflector M; Comas et al., 1992; Chalouan et al., 1997). The base of Pliocene–Pleistocene seismic Unit I, imaged in the seismic profiles as a prominent channeled, erosional unconformity, correlates with the top of the Messinian evaporite sequence recognized throughout the Mediterranean (the "M-reflector" of Ryan, Hsü et al., 1973; Cita and McKenzie, 1986; Comas, Zahn, Klaus, et al., 1996).

Available data indicate that the acoustic basement beneath the Alboran Sea is heterogeneous, formed of either metamorphic or volcanic rocks. Metamorphic rocks of the Betic and Rif Chains have been recovered at the bottom of commercial wells offshore Spain (Fig. 3) and DSDP 121 data predicted the basement high drilled during Leg 161 to be formed of metamorphic rocks (Kornprobst, 1973; Ryan, Hsü et al., 1973; Steiger and Frick, 1973). East of 4º W, most of the residual highs sampled by dredging (Gierman et al., 1968; Mauffret et al., 1987) and diving (Comas et al., unpubl. data) appear to consist of volcanic rocks (Fig. 4). Notwithstanding, the nature of the true basement in the eastern Alboran region is still unknown, because volcanic edifices may overlie older sediments in places.

The structural pattern of the Alboran Basin is currently explained as resulting from the aftermath of two consecutive stages of extensional (early Miocene to early–late Miocene) and contractional (Late Miocene to Holocene) tectonics (Comas, 1996). Shallow structures imaged in multichannel seismic reflection profiles include extensional and later compressional/contractional structures (Fig. 4). Two main episodes of extensional faulting (rifting), Burdigalian–Langhian (about 17–15 Ma) and Serravallian–early Tortonian (about 14–9 Ma), have been identified; the middle to early–late Miocene volcanism and mud diapirs in the basin are thought to be related to this extension (Comas et al., 1992, 1997; Watts et al., 1993; Chalouan et al., 1997; Pérez-Beluz et al., 1997). Tectonic-subsidence analyses (backstripping of commercial well data in the Spanish margin; Watts et al., 1993; Docherty and Banda, 1992, 1995) estimate that rapid extension (initial rifting) continued during the early and middle Miocene, which is in accord with the seismic data. Deep structures in the basement are imaged from deep-seismic reflection profiles in the northern half of the Alboran Basin, which have been interpreted as extensional shear-zones, associated with major extensional detachments in the Betic Chain (Watts et al., 1993; Comas et al., 1997).

Seismic images suggest that rifting was completed in the late Tortonian; after that, a compressional/contractional regime affected the whole basin (Mauffret et al., 1987, 1992; Bourgois et al., 1992; Maldonado et al., 1992; Comas et al., 1992; Watts et al., 1993; Morel and Meghraoui, 1996; Chalouan et al., 1997; among others). Axes of compression appear to have been similar to those described above from the inland regions (e.g., Woodside and Maldonado, 1992). Seismic Units III (late Tortonian), II (Messinian), and I (Pliocene–Pleistocene) are generally interpreted as postrift sediments (Comas et al., 1992; Chalouan et al., 1997). Pliocene and Pleistocene structures accounted for noticeable submeridian contraction and roughly east-west transtension in the marine basin; coevally, general uplifting and emersion at the basin margins (i.e., in the Betics and Rif) is noticeable (Morel, 1989; Rodríguez-Fernández and Sanz de Galdeano, 1992; Sanz de Galdeano and Vera, 1992; Morel and Meghraoui, 1996). The subsidence history at these times has been considered either thermal or flexural (Docherty and Banda, 1992; Watts et al, 1993; Docherty and Banda, 1995). Contemporaneous global oceanography and related sea-level changes further influenced the post-Messinian paleogeographic evolution of the region into the present configuration of the Alboran Sea.

Geophysical Constraints

Geophysical data have provided constraints on the regional crustal thinning and configuration from the surrounding chains to the Alboran Sea. Seismic refraction data and gravity modeling indicate an abrupt change in crustal thickness from about 35–36 km in the Internal Zones of the Betic and Rif Chains to 15–20 km beneath the Alboran Sea (Hatzfeld, 1976; Banda and Ansorge, 1980; Medialdea et al., 1986; Torné and Banda, 1992; Banda et al., 1993; Watts et al., 1993; Galindo-Zaldívar et al., 1997). Heat-flow data suggest a dramatic eastward decrease in mantle lithosphere thickness (60–90 km to about 35–40 km) and concurrent crustal thinning (14–16 km to 10–12 km) from the West Alboran Basin to the transition of the East Alboran Basin to the South Balearic Sea (Polyak et al., 1996). Furthermore, recent 3D modeling (Torné et al., unpubl. data) suggests that variations in crustal thickness span from 36 km (underneath the Betic and Rif Chains and the Gibraltar Arc region) to less than 10 km in the easternmost Alboran Basin; the concurrent mantle lithosphere thickness varies from 140 km to less than 40 km. Neither geophysical nor geological evidence of Cenozoic oceanic lithosphere exist in the Betic-Rif-Alboran region. Multichannel deep-seismic data, however,

point to the presence of oceanic crust east of 1ºW meridian in the South Balearic Basin (Comas et al., 1997).

Various positive gravimetric anomalies along the coast (Bonini et al., 1973) appear to be associated with the Ronda and Beni-Busera mantle peridotite massifs, the largest exposure worldwide of subcontinental lithospheric mantle. The origin of these bodies has been the subject of considerable debate, as they have been interpreted as being deep-rooted (Bonini at al., 1973; Weijermars, 1985); field evidence, however, indicates they form a sheet interleaved within crustal rocks (Lundeen, 1978; Tubía and Cuevas, 1986; Balanyá and García-Dueñas, 1987; Sánchez-Gómez et al., 1995), which is further supported by gravity modeling (Torné et al., 1992). The aeromagnetic anomaly map shows a pattern of volcanic ridges, particularly in the central and eastern Alboran Sea (Galdeano et al., 1974).

The mantle beneath the Alboran Basin shows a zone of low *P*-wave velocity and seismic wave attenuation (around 7.6–7.9 km/s; Hatzfeld, 1976; Banda et al., 1993). Seismological studies in the central and eastern Alboran Sea indicate that this attenuation zone coincides with a gap in intermediate-depth seismic activity, notably at relatively shallow depths (60–20 km; Seber et al,. 1996), which probably indicates either that the upper-lithosphere mantle is hot enough to behave plastically, or the presence of upwelled asthenospheric material at subcrustal depths. However, significant subcrustal and intermediate-depth seismic activity (depths up to 150 km) occurs beneath the western Alboran Sea and the Betic and Rif regions (Seber et al., 1996; Mezcua and Rueda, 1997; Morales et al.,1997). The occurrence of deep earthquakes beneath southern Spain (depths up to 640 km; Grimison and Chen, 1986; Buforn et al., 1991, 1995) and tomographic images suggest the presence of seismically active, high-velocity upper-mantle material beneath the low-velocity, high-attenuation zone. This material has been interpreted as a sinking detached slab from a former subducted lithosphere (Blanco and Spakman, 1993) or as a delaminating continental lithosphere body (Seber et al., 1996; Mezcua and Rueda, 1997).

DRILLING OBJECTIVES

The prime tectonic goal of Leg 161 was to investigate processes that could explain the origin of the Neogene, late orogenic, extensional basins that developed behind highly arcuate thrust belts in the western Mediterranean. The highest drilling priority, therefore, was to sample the basement of the Alboran Basin to test proposed models of basin formation.

Precise tectonic objectives centered on:

1. The age, rate, and thermal history of the extension beneath the Alboran Sea and the timing and role of magmatism and volcanism during extension. The pressure-temperature histories and absolute ages of predicted metamorphic basement rocks were expected to provide constraints on the initial thermal structure, the exhumation and denudation history, and the processes that have modified the crust since the initiation of extension.
2. The rifting geometry that caused crustal thinning in the region. Drilling results combined with on-land structural data and seismic profiling information at sea were anticipated to discriminate between prevailing rifting models. Furthermore, we planned to compare total and tectonic subsidence from drill sites with subsidence curves computed for the commercial wells on the Spanish and Moroccan margins in order to constrain the magnitude and timing of rifting.
3. The postrift deformation of the basin. By sampling syndeformational sequences we sought to establish the timing and to test the contractional reorganization of the basin and, where volcanic rocks were sampled, the role of magmatism at this stage.

To address these topics within a single leg, during which both tectonic and paleoceanographic objectives had to be allocated, three of the proposed drill sites (Alb–2A, Alb–4A, and Alb–3A) were originally chosen as prime sites. Alb–2A in the West Alboran Basin became Site 976 (Figs. 2, 4), at which we expected, and were able, to penetrate through the sediment cover and recover hard rock samples at least 200 m down into the basement. Alb–4A in the East Alboran Basin became Site 977 (Figs. 2, 4), at which we expected to sample the sedimentary cover to the granted total depth of 1200 m; however, we failed to do so because the drill pipe became stuck at a slightly over-pressured conglomerate level and drilling was terminated at 598.5 mbsf (Fig. 3). Trying to penetrate and sample sediments below the conglomerate level encountered at Site 977, we then drilled at Site 978 (originally Alb–4B and the alternative for Site 977), located at an equivalent position in the East Alboran Basin, only a few km to the north (Fig. 2). Unfortunately, at Site 978 we were once again unable to penetrate and sample as deep as projected (1400 mbsf). Drilling was terminated at 698.0 mbsf, just 100 m deeper than at Site 977, because of an unsuccessful attempt to re-enter the same hole through the deployed FFF (Free Fan Funnel) after a change of drill-bit. Site 979 (former Alb-3A) was then drilled to penetrate a tilted Pliocene–Pleistocene sequence in the South Alboran Basin (Figs. 2, 4); coring and logging at this site ended *JOIDES Resolution* drilling operations during Leg 161.

SITE BY SITE RESULTS

This section summarizes the results from the four drill sites of Leg 161 (Figs. 2–4) that aid in better understanding the tectonic history and origin of the Alboran Basin.

Site 976 (West Alboran Basin)

Site 976 (Shipboard Scientific Party, 1996b) was drilled in the West Alboran Basin. It is about 110 km east of the Strait of Gibraltar and 8 km northeast of DSDP Site 121, drilled during Leg 13 in 1970 (Ryan, Hsü et al., 1973). A seismic survey (Klaus and Shipboard Scientific Party, 1996) was carried out from *JOIDES Resolution* to verify site location and Site 976 drilled at the intersection of *JOIDES Resolution* single-channel seismic profiles and MCS line ALB-39 (Fig. 2), 8 km northeast of DSDP Site 121 (see Fig. 16, on the back-pocket foldout, this volume). Site 976 lies on a basement high correctly predicted as being formed of metamorphic rocks exhumed during the rifting; it composes the most prominent crustal structure in the Alboran Basin (Fig. 4). The basement was penetrated to a maximum depth of 260 m at Hole 976B and to 85 m at Hole 976E. A total of 343.19 m of high-grade metamorphic rock was cored in the two holes (Figs. 3, 5), averaging 27.8% recovery of hard rocks.

A full suite of logging tools was run in Holes 976B and 976E (quad-combo, FMS, BHTV, and geochemical), yielding information on unrecovered intervals, on the basement/sediment transition in Hole 976B, and on fault-gouge zones within the basement. Thermal gradient and in-situ sediment conductivity measurements from logging (ADARA and water-sampling temperature probe [WSTP] data), conducted in both holes, indicated a heat-flow of 102 mW m^{-2}, which is in good agreement with average heat-flow values in the West Alboran Basin (Polyak et al., 1996).

The Sedimentary Cover

Age Constraints and Subsidence

Drilling in Holes 976B and 976E sampled the entire sedimentary cover above the metamorphic basement in a sector wherein seismic images suggest that Messinian seismic Unit II is practically absent. The stratigraphic sequence consists of 650 m of late Serravallian to

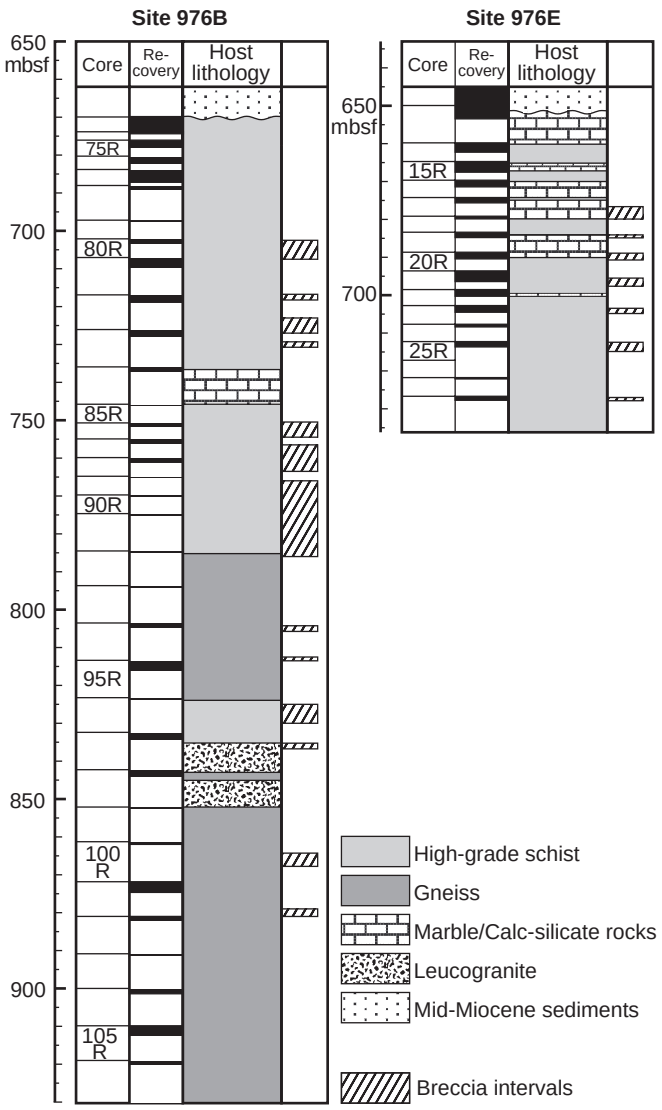

Figure 5. Basement sections in Holes 976B and 976E showing recovery and sampled metamorphic rock types (from Shipboard Scientific Party, 1996b). Main intervals of brittle deformation (breccia and fault-gouge intervals) deduced from core description and logging characteristics are indicated by shaded bands on the right-hand side of each lithologic column (from Comas and Soto, Chap. 25, this volume).

Holocene marine sediments (Fig. 3), including hemipelagites, and muddy turbidite and gravity-flow facies (Alonso et al., Chap. 4, this volume). The Miocene/Pliocene boundary is ~572 mbsf, and the Pliocene Pleistocene boundary is about 360 mbsf. On the basis of new biostratigraphic data (from Nannofossil Zones [NN]), Siesser and de Kaenel (Chap. 16, this volume) refined the ages of the two major hiatuses identified in the sedimentary sequence in Hole 976B by Shipboard Scientific Party (1996b). They determined that the hiatuses are within the late Miocene (lower Tortonian [NN9 to NN10], from about 10.2 Ma to 8.6 Ma;) and between the early Pliocene and late Pliocene (Zanclean and Piacenzian [NN13 to NN16] from about 5 Ma to 2.5 Ma). The late Tortonian and Messinian? (NN11) and earliest Pliocene (NN12) intervals, according to these authors, have a total thickness of about 66 m and 57 m, respectively; they consist of open-marine fine-grained sediments. Average sedimentation rates are low for the late Miocene (15 m/m.y.), and particularly high for the earliest Pliocene (453 m/m.y.), late Pliocene (340 m/m.y.), and Pleistocene–Holocene (208 m/m.y.; Shipboard Scientific Party, 1996b).

In both holes, uppermost Serravallian marine deposits (NN7, 11–12 Ma) overlie the brecciated basement (lithostratigraphic Unit IV; Shipboard Scientific Party, 1996b). In Hole 976B, the basal sediments (lithostratigraphic Unit IV, equivalent to seismic Unit IV; Fig. 3) consist of interspersed pebbles to sand-sized clasts of metamorphic rocks, similar to the underlying basement lithologies, with mixed deep- and shallow-water fauna. In Hole 976E, basal sediments above the basement are formed of a 15-cm-thick sandy-silty claystone interval. The Serravallian sand includes significant volcanic components, as deduced from a high plagioclase content, relict pyroclastic textures in sand grains, and a high percentage of zeolite alteration minerals. It has therefore been interpreted as epiclastic deposits likely associated with a previous or near-coeval pulse of volcanism in the basin (Marsaglia et al., Chap. 3, this volume).

Subsidence analyses (Fig. 6) at Site 976 and at two commercial wells (Granada-D1 in the Granada Basin, and Andalucía-A1, Fig. 4; see Fig. 18, on back-pocket foldout, this volume) provide some constraints on the subsidence and uplift history across the basin (Rodríguez-Fernández et al., Chap. 5, this volume). The backstripped diagram at Hole 976B has been calculated using porosity, density, sedimentary, and biostratigraphic data from Shipboard Scientific Party (1996b); backstripping at the commercial wells consider paleobathymetric corrections from new sedimentary and biostratigraphic studies on well samples. Steep sections of the diagram at Site 976 reveal two sudden periods of subsidence in the late Serravallian (from 11 to 10.7 Ma) and during the late Pliocene and Holocene (from 2.5 Ma onwards), and uplift of the metamorphic basement high during the late Pliocene (from 5 to 2.5 Ma). According to these results, total subsidence at Site 976 is on the order of 900 m during the late Serravallian (subsidence rate of about 3 km/m.y.) and on the order of 1200 m during the late Pliocene to Holocene (subsidence rate of about 480 m/m.y.).

Seismic Reflection and Logging Analysis

In order to maximize drilling results, regional seismic reflection data from the vicinity of Site 976 have been pooled for postcruise research. To this end, seismic analyses have been carried out on the *JOIDES Resolution* lines (Lines 2S-1 and 2S-2) and MCS reflection profiling (5–8 s, TWT penetration) around Site 976 (Figs. 4, 7, 8; see Fig. 16, on back-pocket foldout, this volume).

Wireline logging and biostratigraphic data from Hole 976B have been tied to *JOIDES Resolution* line 2S-1 by synthetic seismograms (Tandon et al., 1998). This study has distinguished several key reflectors within the sedimentary cover: the boundaries between seismic Subunits Ia (Pleistocene–Holocene), Ib (late Pliocene), and Ic (early Pliocene), and reflectors M and R3 (Figs. 3, 7).

The structural map in Figure 4, drawn from a dense grid of MCS lines, shows the complex structural pattern of the Alboran Basin, comprising extensional and contractional features. Interpreted MCS reflection profiles cutting across the entire basin are presented in the back-pocket foldout (see Figs. 16 to 19, back-pocket foldout, this volume). The structural high (referred to as the Site 976 High hereafter) is located in a fault-bounded basement forming a rounded-arrowhead outline pointing west. It trends northeast-southwest at the site position, turning northwest-southeast toward the south and east-west toward the north (Fig. 4). The whole length of its convex flanks is normal-faulted, bounding a complex graben filled with lower Miocene (seismic Unit VI, late Aquitanian?–Burdigalian, 22?–19 Ma) to Pleistocene sequences. The shape of the entire graben, which comprises the main depocenter in the West Alboran Basin and a northern prolongation flanking the Spanish shelf, is also arcuate, paralleling the trend of the Site 976 High from southeast of Almería to the Xauen Bank (Fig. 4). Remarkably, this main depocenter is the only one in the Alboran Sea basin in which the basal seismic Unit VI occurs (Fig. 4; Figs. 16, 17, on back-pocket foldout, this volume). In those areas where seismic Unit VI reaches its maximum thickness, that is, in the central West Alboran Basin, an extensive province of mud diapirs has

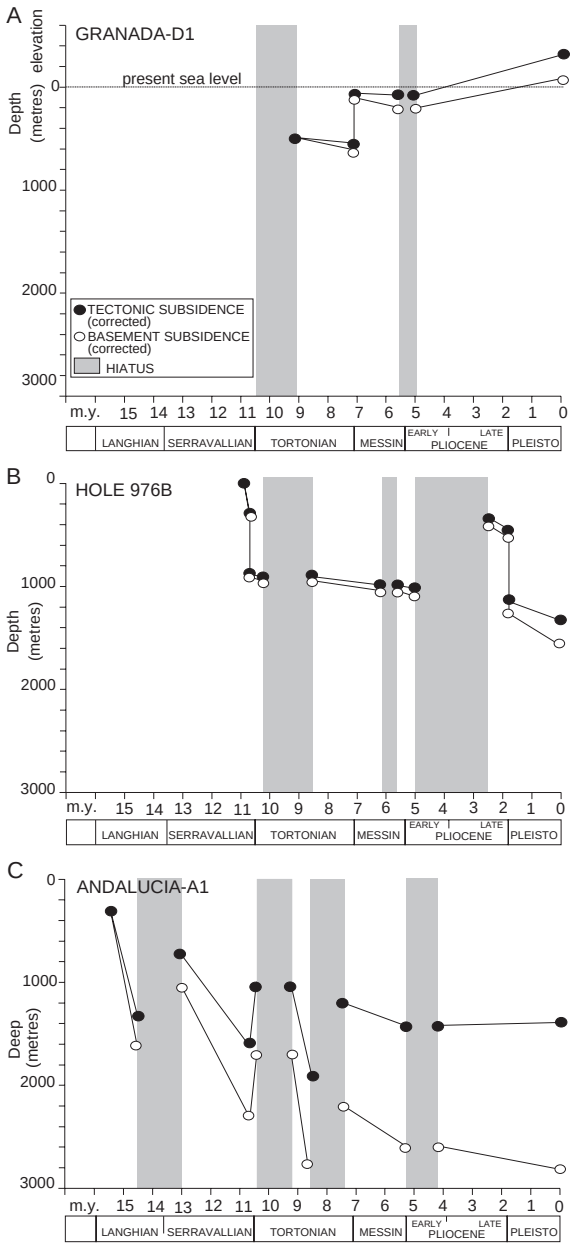

Figure 6. Tectonic and total subsidence plots for the Granada-D1 well (in the Granada Basin [GB], Fig. 4), Hole 976B, and the Andalucía-A1 well, obtained using "backstripping" techniques that consider paleobathymetric corrections (from Rodríguez-Fernández et al., Chap. 5, this volume). The Site 976 High shows two periods of rapid subsidence, at ~11–10.7 Ma (late Serravallian), and at ~1.7 Ma (earliest Pleistocene), and uplift at 5–2.5 Ma. The Andalucía-A1 well shows three periods of subsidence at 15.5–14.5 Ma (Langhian), at 13–10.7 Ma (Serravallian), and at ~9.2–8.5 Ma (Tortonian). The middle to late Miocene steeps in the subsidence curves at Site 976 and the Andalucía A1 well are interpreted as phases of synrift subsidence. Early Pliocene uplift and earliest Pleistocene rapid subsidence at Site 976 could be related to tectonic events during the post-Messinian contractive reorganization of the basin, as the subsidence probably related to episodic transtensional conditions within a general trend of probably thermal, gentle subsidence. The Granada-D1 well shows rapid uplift at the early Messinian (about 7 Ma) followed by an overall negative subsidence trend, indicating that uplift at the basin margins and isolation of the intramontane Betic Neogene Basins started by the latest Tortonian. The general changeover from marine to continental basins is shown at 4 Ma (early Pliocene). Location of wells is shown in Figures 2 and 4; drilled sequences are shown in Figure 3.

developed. According to seismic images, the diapirism began by the middle Miocene and large diapirs occupy a huge part of the depocenter; the diapirs are rooted in the basal olistostromic seismic Unit VI. Diapirism likely resumed by the Pliocene and the top of some diapirs then reached nearly to the seafloor (Comas et al., 1992, 1993; Maldonado et al., 1992; Pérez-Belzuz et al., 1997).

In the northern branch of the major-graben depocenter (hereafter called the Málaga Graben; Figs. 4, 8–10; Figs. 16 and 17 on back-pocket foldout, this volume) sediments attain up to 5 km in thickness just facing the drill site (according to depth conversions); notably, toward the southwest, sediment thickness is up to 7–8 km in the center of the West Alboran Basin and up to 4 km to the south near Xauen Bank in the southern Alboran Sea (Soto et al., 1996; Chalouan et al., 1997).

The contour map of the top of the basement (Fig. 10) reveals the complex and structurally asymmetric character of the Málaga Graben. Both flanks of the graben correspond to intricate interference of former submarine or formerly emerged surfaces, and low- and high-angle normal faults, oblique transfer faults, and tops of rollover structures affecting the basement (de la Linde et al., 1996). Seismic section across the Málaga Graben through Site 976 (Fig. 8; Fig. 16 on back-pocket foldout, this volume), and further to the east (Fig. 17, on back-pocket foldout, this volume), show that individual reflectors within the sedimentary cover diverge with different attitude toward the steeply dipping border faults, indicating that faulting was active at both flanks of the graben at somewhat different times. At places, the contact between the sedimentary cover and the basement likely accommodated normal faults (Figs. 7, 8; Fig. 16 on back-pocket foldout, this volume). The seismic images suggest that the northern flank of the graben was relatively uplifted at some time between the late Tortonian (age of reflector R3) and the Pliocene, as Pliocene sediments overlie middle Miocene deposits (seismic Unit IV) near the Spanish coast.

Comas and Soto (Chap. 25, this volume) interpret the structure in the northern flank of the Málaga Graben (Fig. 10; Fig. 16 on back-pocket foldout, this volume) as likely comprising horsetail faults of a listric-fan rooted on deeper listric (intra-crustal) detachments (oriented with the top to the south-southeast), considering that the controlling low-angle master fault (southeast-dipping detachment system) is located in the northern basement slope of the graben. These authors suggest that the Site 976 High has derived from a initial (early Miocene) rollover anticline, subsequently faulted by counter faults, therefore representing a central high (following Gibbs, 1984) in the Alboran Basin.

Single-channel Line 2s-1 (Fig. 7) images normal faulting on the crest and flanks of the Site 976 High, consistent with data indicating brittle deformation of the basement (see below). In the northwest flank of the high, individual reflectors within sediments of seismic Unit IV are synsedimentary normal faulted, confirming that extension continued till the middle Miocene, as demonstrated by drilling (Langhian age of lithostratigraphic Unit 4; Shipboard Scientific Party, 1996b). According to seismic images, Messinian Unit II is missing at the top of the basement high and further to the southeast. The M-reflector, either an erosional or nondepositional surface, correlates with the base of early Pliocene seismic Subunit Ic (Tandon et al., 1998). The anticline attitude of Miocene and early Pliocene (seismic Subunit Ic) sediments, as well as the unconformity at the top of Subunit Ic, indicate that the whole packet (basement through Unit II) was upwarped during Subunit Ic times (i.e., during the early Pliocene).

Statistical measurements on processed FMS and BHTV electrical images from Hole 976B (de Larouzière et al., Chap. 24, this volume) indicate that low-angle surfaces within the basement, probably representing the metamorphic foliation, tend to dip to the west; steeper surfaces, interpreted as brittle fractures or faults, are mostly east dipping. Narrow intervals with sharp changes in hole geometries can be ascribed to active faults, also recognizable in BHTV images. Mapping of these faults (up to 20 active faults at Hole 976B) leads de Larouzière et al. (Chap. 24, this volume) to propose a present-day stress re-

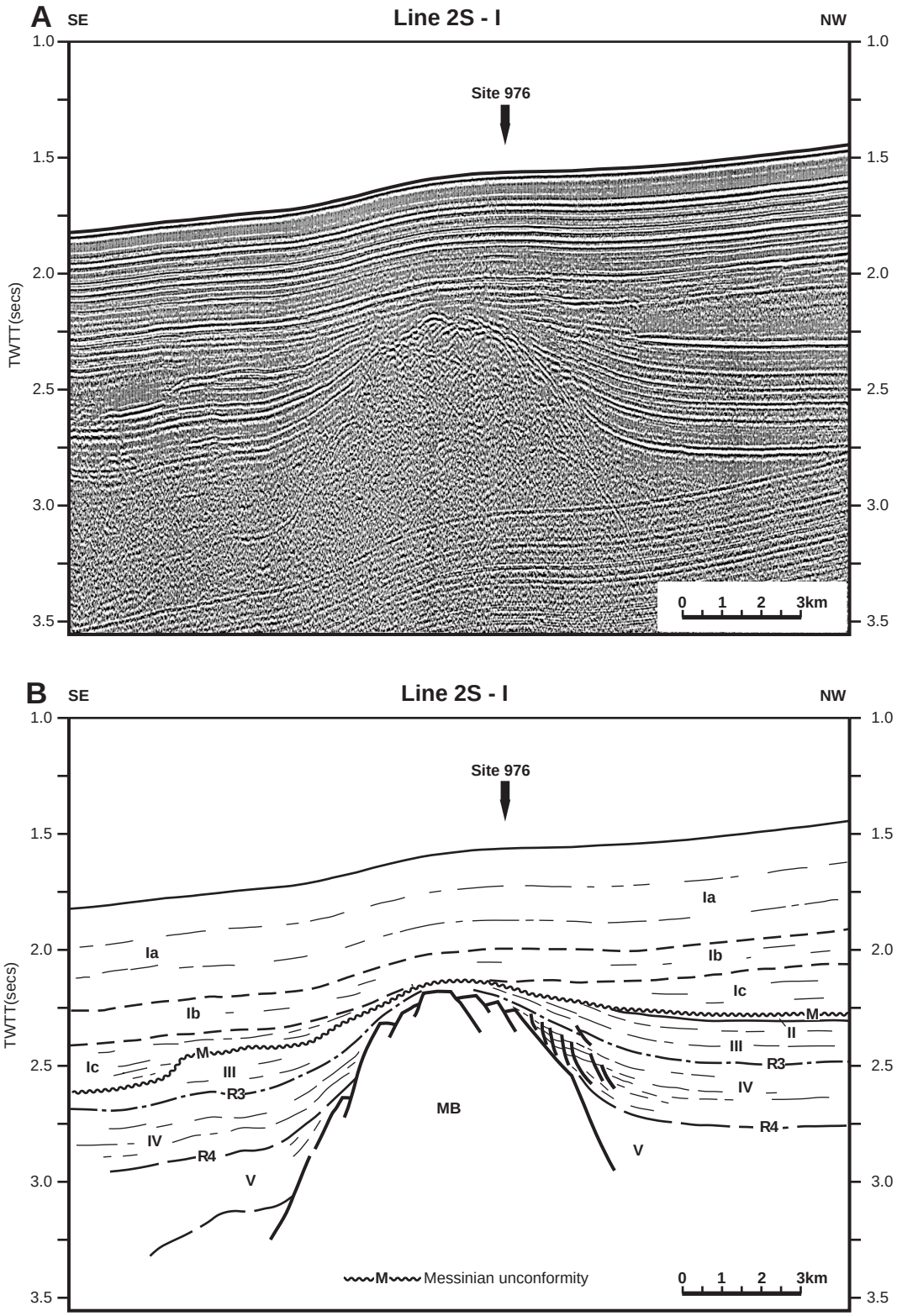

Figure 7. *JOIDES Resolution* seismic Line 2S-I (single channel) across Site 976. **A.** Original profile. **B.** Draw-line interpretation of Line 2S-I based on Site 976 data (modified from Shipboard Scientific Party, 1996b). Reflectors and seismic units as in Figures 3 and 15. MB = Metamorphic basement. Location of seismic line is shown in Figure 2. See text explanation.

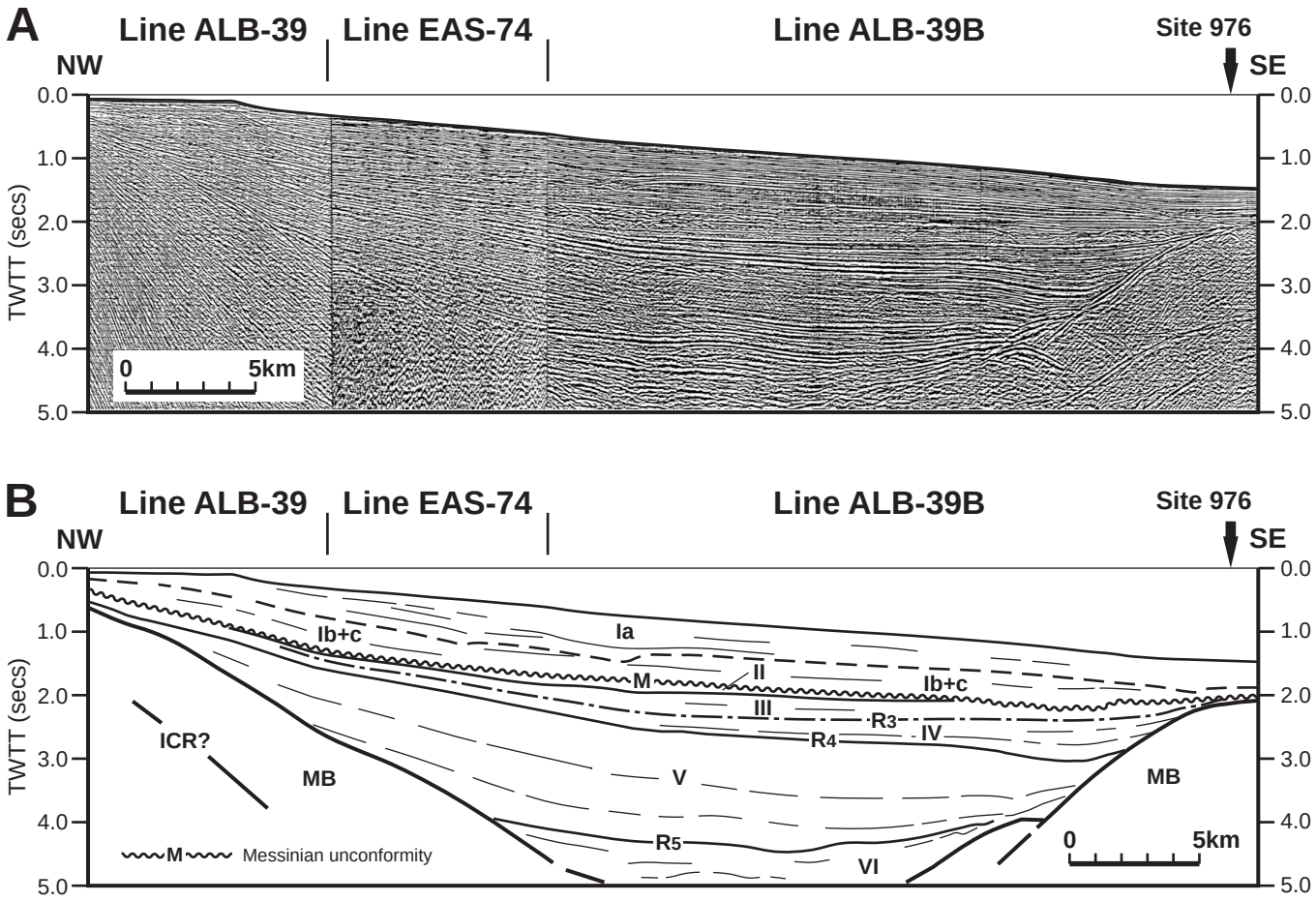

Figure 8. **A.** Composite profile from multichannel seismic reflection lines ALB-39, EAS-74, and ALB-39B across the Málaga Graben and the Site 976 basement high. **B.** Draw-line interpretation of multichannel seismic reflection profile in (A). Note that attitude of individual reflectors indicates diachronic normal faulting bounding the graben. The top of the basement probably corresponds to low-angle normal faults. Reflectors and seismic units as in Figures 3 and 15. MB = Metamorphic basement. Location of seismic line is shown in Figure 2.

gime in the area with a relative east-west direction of extension (maximum stress direction σ_1 is near vertical and minimum stress direction σ_3 strikes N80°E).

The Metamorphic Basement

Basement Lithologies

The upper 124 m of cored basement at Hole 976B consists of biotite-sillimanite-plagioclase high-grade schist, with visible porphyroblasts of garnet and andalusite. This metapelite sequence has interlayered calcite and dolomite marble and associated calc-silicate rocks as reaction bands, which developed along the metapelite-metacarbonate contacts (López Sánchez-Vizcaíno and Soto, Chap. 18, this volume). Metacarbonate and associated rocks are particularly abundant in the upper part of the cored section (Fig. 5). This metapelite sequence overlies banded pelitic gneiss with large porphyroblasts of coarse-grained K-feldspar, cordierite, and andalusite. Much of the gneiss is migmatitic, with centimeter-thick veins and segregations of weakly foliated or unfoliated felsic material (leucosomes) containing large crystals of cordierite, biotite, andalusite, and sillimanite. The facts that leucosome geometries largely follow pre-existing planes of anisotropy, that the volume of leucosome veins (<20%) is low with respect to the whole rock volume, and that the common occurrence of mafic selvages (melanosomes) are associated with them, suggest that the low degree of melting was controlled by strong, compositional foliation (Soto and Platt, in press).

Major and trace compositional trends of the gneiss are similar to those of the high-grade schist (Spadea and Prosser, Chap. 28, this volume), indicating a local source for melting and relatively low mobility of melts during migmatite formation (Soto and Platt, in press). Both rock units are cut by peraluminous, leucogranitic dikes. The high-grade schist and the gneiss show differences in their petrological and structural evolution; at Hole 976B, they are separated by a significant fault zone (Fig. 5), according to BHTV and FMS images (Comas and Soto, Chap. 25; de Larouzière et al., Chap. 24, both this volume).

Two systematically identifiable sets of ductile fabrics and structures can be distinguished in the high-grade schist, referred to as D_1 and D_2 by Shipboard Scientific Party (1996b). The earlier fabric, S_1, is characterized by compositional layering and biotite-rich laminae and oriented biotite. S_1 has been intensively affected by 1–50 mm-scale tight, asymmetrical D_2 folds. Biotite is recrystallized in the fold hinges and tends to lie parallel to the axial surface, as do elongated mats of fibrolite, the two together defining an axial planar fabric, S_2. In much of the high-grade schist, D_2 has been so strong that the main foliation is in fact a composite fabric formed by the transposition and modification of S_1. D_2 was followed by static crystallization of andalusite, plagioclase, a second garnet, and K-feldspar. The gneissic

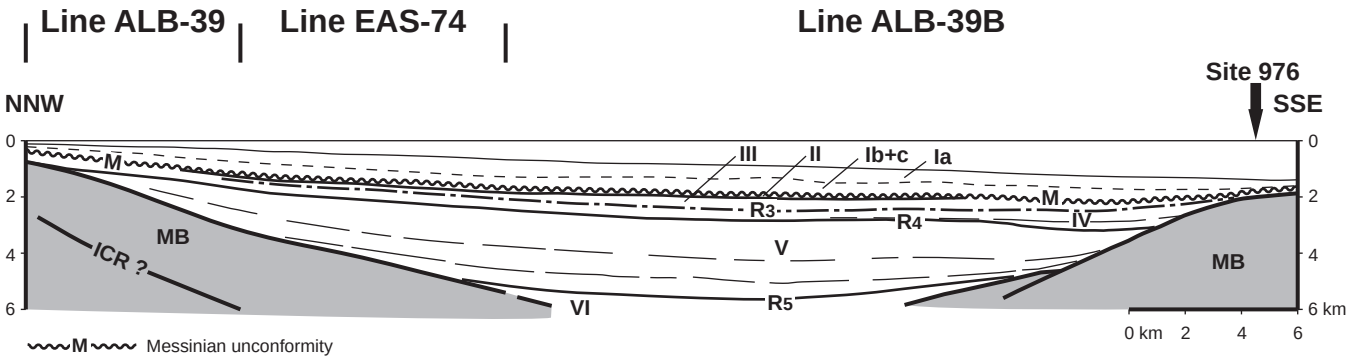

Figure 9. True-scale cross section from seismic lines shown in Figure 8. Depth conversion is from stack velocity analysis in seismic reflection. Numbers = lithoseismic units from Figures 3 and 15. MB = Metamorphic basement.

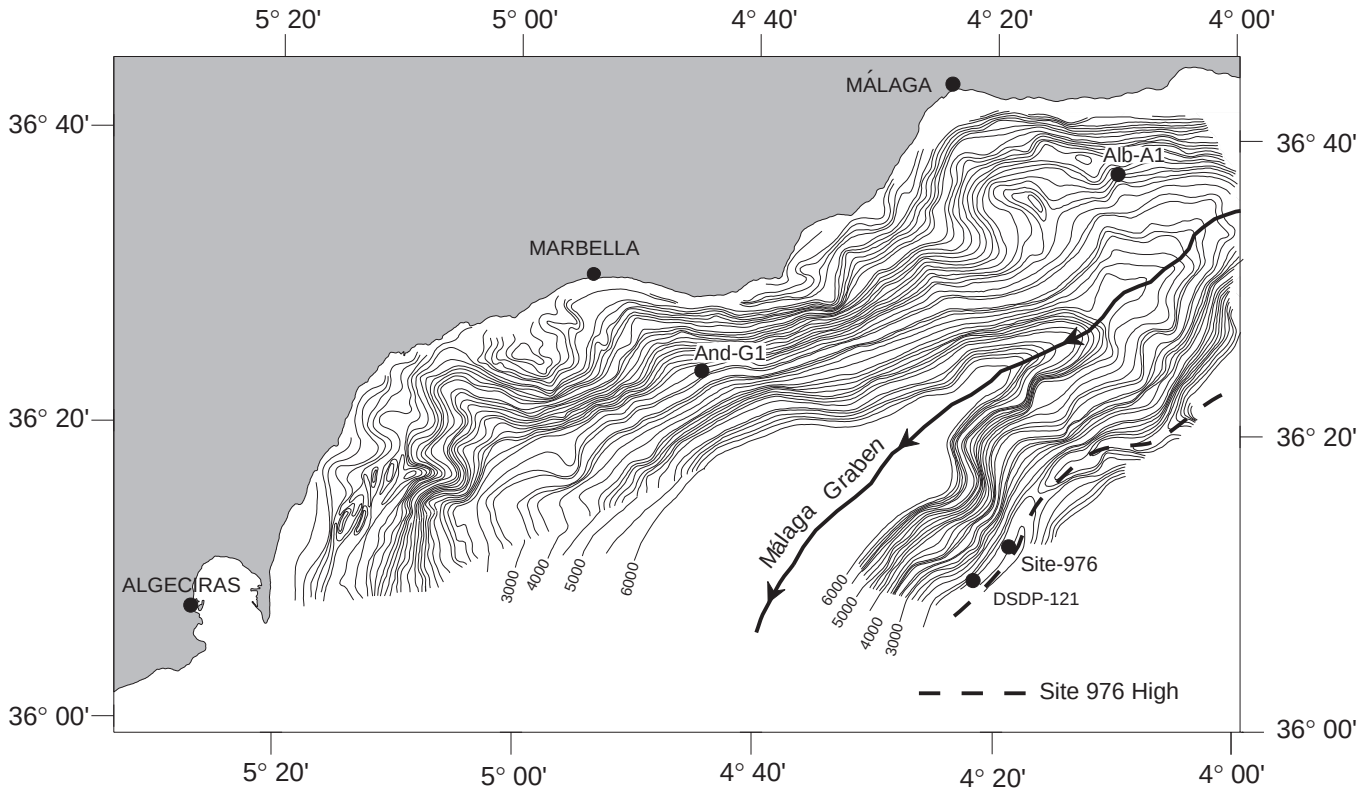

Figure 10. Basement depth contour map of the Málaga Graben (de la Linde et al., 1996). Contour lines every 100 ms (TWT), showing Andalucía-G1 (And-G1), Alborán-A1 (Alb-A1), DSDP 121, and Site 976 locations. Both flanks of the graben correspond to complex interference of former submarine or formerly emerged surfaces and low- and high-angle normal faults, normal-oblique transfer faults, and tops of rollover structures affecting the basement. Steep surfaces near the Spanish coast correspond to post-Messinian strike-slip or oblique faults that prolongate on land.

foliation in relation to the deformational history of the schist is uncertain. On the basis of textural relationships, it is a composite foliation, which may have initially formed at about the same time as D_2 in the high-grade schist but was subsequently heavily modified by compaction or further deformation during partial melting (Soto and Platt, in press).

Metamorphic P-T-t Evolution

The P-T-t evolution of the high-grade schist and gneiss is shown in Figure 11A (Soto and Platt, in press). The most complete mineral assemblages in these rocks are:

1. Fe-rich high-grade schist: Biotite + Garnet ± Staurolite + K-feldspar + Fibrolite ± Andalusite + Plagioclase + Rutile + Ilmenite + Quartz;
2. Al-rich high-grade schist: Biotite + Garnet + Corundum + Fibrolite + Andalusite + K-feldspar + Plagioclase + Ilmenite; and
3. Gneiss: Biotite + Cordierite ± Garnet + Fibrolite + Andalusite + K-feldspar + Plagioclase + Ilmenite + Magnetite + Quartz.

As reaction textures among the mineral phases, and in particular between andalusite and sillimanite, are always present in the rocks, the above-mentioned mineral assemblages should be considered dis-

equilibrium assemblages. Nevertheless, the high-grade schist assemblage reflects lower peak-temperatures than the gneiss assemblage. Thermobarometric estimates on the high-grade schist give approximate P-T conditions of 3.5–5.5 kbar at 650°–700° C for the matrix assemblages (Soto and Platt, in press; Prosser et al., Chap. 20, this volume). The gneiss achieved higher temperature during its metamorphic evolution, with approximate melting conditions of 700°–750°C, at 6 kbar to 3 kbar (Soto et al., Chap. 19, this volume).

The first stages of the P-T evolution of the high-grade schist are only preserved in the cores of garnet porphyroblasts and are characterized by prograde evolution through the temperature range 500º–600°C, accompanied by a slight drop in pressure, from 10.5 kbar to 8 kbar. Subsequently, the main deformation event took place along a decompression P-T path, concomitantly with a temperature rise, achieving final conditions of 650º–700°C and 3–4 kbar. Overall, a temperature increase of 50°C to 100°C occurred during decompression, from more than 8 kbar to less than 4 kbar (Soto and Platt, in press).

The decompression P-T paths of the high-grade schist and gneiss were followed by a cooling path of up to T < 500º–600°C and P < 2–3 kbar. During this evolution, crystallization of residual granitic melts occurred under overstepped conditions in the andalusite stability field. Ar/Ar dating on muscovite and biotite indicates that cooling took place at 20.0 ± 0.2 Ma (±2σ) for muscovite and 19.2 ± 0.7 Ma (±2σ) for biotite (Kelley and Platt, Chap. 22, this volume). Apatite fission-track analyses on the same rocks indicates cooling below the apatite partial annealing zone (60°–120°C) at 18.3 ± 1.0 Ma (± 2σ; Hurford et al., Chap. 21, this volume). All these data suggest that during the early Miocene the basement cooled rapidly from 426 ± 22°C (the estimated closure temperature of muscovite) to 60°C in a period of between 0.5 m.y. and 2.9 m.y., which gives an average minimum cooling rate of 126°C/m.y.

Results of Thermal Modeling

Platt et al. (in press) present the results of thermal calculations carried out to explain the P-T path determined by Soto and Platt (in press) for the high-grade schist sampled at Site 976. As mentioned above, the essential features of this path (Fig. 11A) are that the rocks reached pressures of up to 10.5 kbar at ~500°C relatively early in their history, corresponding to a burial depth of about 40 km, followed by decompression and heating to a peak temperature of 650º–700°C at a pressure of about 3–4 kbar, and then by cooling at low pressure.

Variables considered in the modeling included the thickness and thermal gradient of the post-orogenic lithosphere, the radiogenic heat production in the thickened crust (assumed to be 60 km thick); the time gap (pause) between the end of contractional tectonics and the start of extension, the effects of convective removal or delamination of lithospheric mantle at depths of 125, 75, or 62.5 km, and the rate of extension.

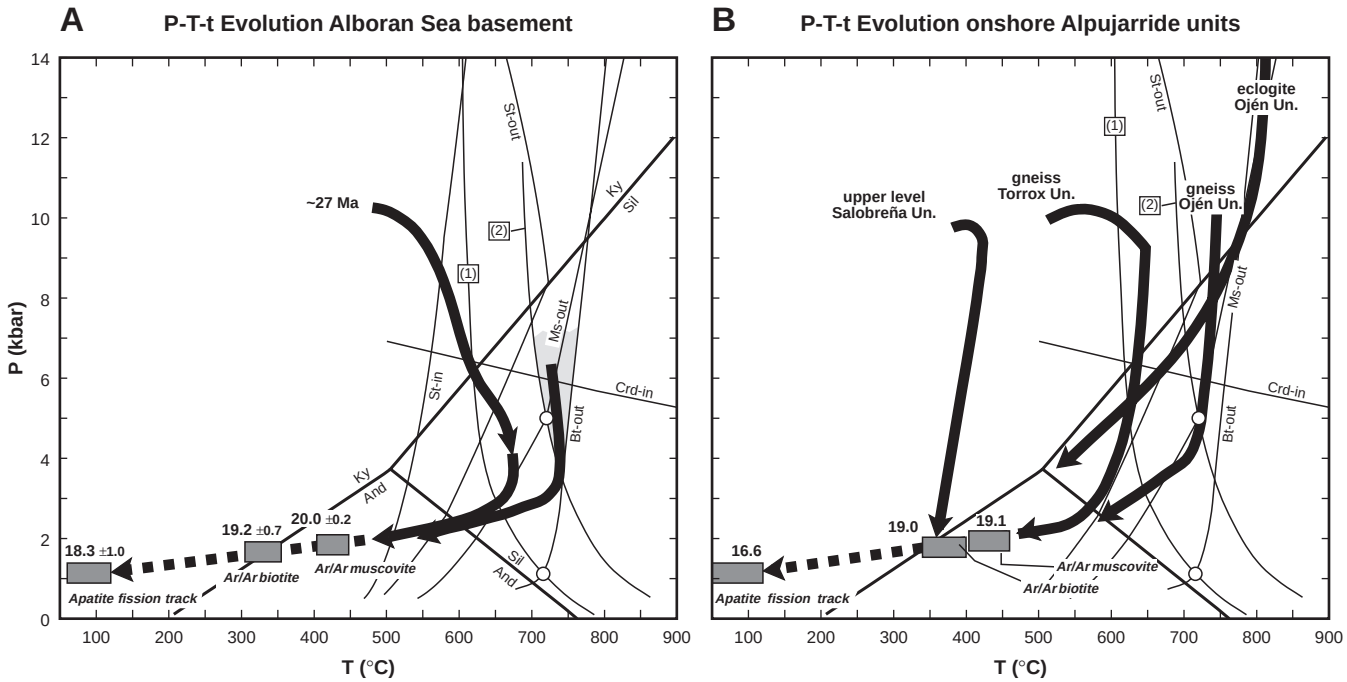

Figure 11. Comparison between the metamorphic P-T-t evolution of the Alboran Sea basement and the P-T evolution experienced by several Alpujarride units from the western Betic Cordillera. **A.** Metamorphic evolution of the high-grade schist and melting conditions in the gneiss (shaded area) at Site 976 (from Soto and Platt, in press). P-T evolution of the migmatitic and pelitic gneiss are from Soto et al. (Chap. 19, this volume). Approximate cooling P-T path is shown by the broken line. Age determinations (± 2σ) along the cooling path correspond to Ar/Ar mean central ages of coexisting biotite and muscovite (from Platt and Kelley, Chap. 22, this volume) and apatite fission track mean ages (from Hurford et al., Chap. 21, this volume). The estimated closure temperature of muscovite (426 ± 22°C) and biotite (330 ± 25°C) are from Platt and Kelley (Chap. 22, this volume). Temperature of the apatite partial annealing zone in these rocks (60–120°C) is from Hurford et al. (Chap. 21, this volume). **B.** Thermal evolution of the different Alpujarride units is from Tubía et al. (1997) for the eclogite rocks of the Ojén Unit (underlying the Ronda peridotite slab), from Sánchez-Gómez et al. (Chap. 23, this volume) for the gneissic rocks of the same unit; García-Casco and Torres-Roldán (1996) for the gneissic rocks of the Torrox Unit, and Azañón et al. (1998) for the upper levels of the Salobreña Unit. Average age determinations have been calculated with the following data sets: Zeck et al. (1992), Monié et al. (1994), Andriessen and Zeck (1996), and Sosson et al. (1998). The P-T grid is composed from Spear and Cheney (1989), Vielzeuf and Clemens (1992), granite solidi sources are summarized in Johannes and Holtz (1996), and Al-silicate triple point from Berman (1988) (for further details see Soto and Platt, in press). (1) = H_2O-saturated granite solidus, (2) = Muscovite + K-feldspar + Quartz + H_2O = Liquid.

The only combinations of variables that produce modeled P-T paths (Platt et al., in press) with the observed characteristics involve high radiogenic heat production combined with a significant post-contractional pause (to produce high temperatures in rocks initially at 40 km depth), removal of mantle lithosphere below 62.5 km (to produce further heating during decompression), exhumation by extension at a very high rate (about 4.5 km/m.y., to delay the onset of cooling until the rocks reached shallow depths), and final exhumation and cooling at a rate of 4 km/m.y. (to satisfy radiometric and petrological constraints). This results in a total time of about 9 m.y. for exhumation from 40 km depth to the surface. Apatite fission-track analysis (Hurford et al., Chap. 21, this volume) indicates that the rocks cooled below 60°C at 18.3 ± 1.0 Ma, so the thermal modeling results suggest that extension started at about 27 Ma.

Brittle Deformation: Breccias and Fault Gouges

Faulting, brecciation, and fracturing characterize a brittle deformation at the top of the basement in both Holes 976B and 976E. Intervals of polymictic breccia and clay-rich fault-gouges in Holes 976B and 976E mark zones of brittle faulting and their widespread occurrence largely determined the low total recovery (Fig. 5).

Comas and Soto (Chap. 25, this volume) report that brittle deformation was mainly a result of fault-related cataclasis, as most of the breccia and fault gouge intervals are cataclasites. The cataclastic breccias consist of consolidated rocks with angular and highly variably sized clasts (<60%) from nearby basement lithologies, a matrix formed by comminution of the metamorphic clasts, and a dolomite-rich cement with abundant displacive and replacive textures. The fault gouges comprise angular fragments of basement rocks in a clay-rich, dark matrix (>70%). Cataclastic structures in breccias and gouges include cataclastic foliation, cataclastic flows, and cataclastic lineation. Extensive internal microfracturing (splintered grains) in metamorphic clasts has been interpreted by these authors as being caused by tectonic extension, decompression and fast exhumation of the metamorphic basement. Open fracturing in breccias is indicated by sediment-fill fractures. Neptunian dikes and sills filled with late Serravallian sediments in the uppermost basement cores from Holes 976B and 976E prove that dilation and brittle tensional fracturing in the top of the basement occurred in a submarine environment. Sediment injections into open fractures and pervasive dolomitization in cataclastic fabrics indicate fluid-assisted processes for brittle deformation, probably including heat advection associated with the tectonic regime (Comas and Soto, Chap. 25, this volume). A major breccia and gouge interval (20–25 m thick) at Hole 976B, coinciding with a noticeable change in basement lithology, corresponds to a thick fault zone separating the higher sequence of high-grade schist and marble from the lower part of the section comprising mainly pelitic and migmatite gneiss (Fig. 5). According to seismic interpretation, this cataclastic zone is probably a westward-dipping brittle fault (Fig. 7).

Sites 977 and 978 (East Alboran Basin)

Sites 977 (Shipboard Scientific Party, 1996c) and 978 (Shipboard Scientific Party, 1996d) were drilled in the East Alboran Basin, south of Cabo de Gata. Site 977 lies the south of Al-Mansour seamount at a secondary depocenter bounded by the Yusuf Ridge, and Site 978 is just 24 km north of Site 977, to the north of Al-Mansour Seamount. Both sites lie in the same east-west–trending, 70-km-wide, main depocenter that connects the Alboran and South Balearic Seas and that opens to the South Balearic Basin (Figs. 2, 4). One single-channel seismic profile (Line 3S; Fig. 12) was acquired by the *JOIDES Resolution* (Klaus and Shipboard Scientific Party, 1996) to verify site location, and Site 977 drilled at the intersection of this line and MCS line Conrad 823 (Fig. 19 on back-pocket foldout, this volume).

Sites 977 and 978 sampled 598.5 m and 485 m, respectively, of equivalent sedimentary sequences. The topmost 213 m of sediments at Site 978 were deliberately washed out (because of the tectonic interest in penetrating as deep as possible), but a continuous sequence from 213 to 698 mbsf of sediments was recovered downhole.

The lowermost fine-grained sediments drilled at Site 977 (at about 530 mbsf) are earliest Pliocene in age (NN-12b; Siesser and de Kaenel, Chap. 16, this volume). Scraping from calcareous cement surrounding pebbles of gravel sampled in the lowermost cores at Site 977 (see below) yielded nannofossil assemblages containing middle and upper Miocene fauna (NN7-NN11; Siesser and de Kaenel, Chap. 16, this volume).

At Site 978, the Miocene/Pliocene boundary is proposed at about 620 mbsf and the lowermost cores at this site, just underlying the gravel interval (see below), have been assigned to the Messinian or latest Tortonian (NN11; Siesser and de Kaenel, Chap. 16, this volume). Iaccarino and Bossio (Chap. 42, this volume) assigned an early Messinian (pre-evaporitic interval) age to foraminifers in these cores. However, they leave open the possibility of early Messinian faunas having been reworked; therefore, they suggest the interval may be latest Messinian in age. The Pliocene/Pleistocene boundary is at about 266 mbsf at Site 977 and at about 223 mbsf at Site 978 (Fig. 3).

A brief early Pliocene hiatus at about 490 mbsf at Site 977 (between 5 and 4 Ma, lasting less than 1.0 m.y.) is reported by Siesser and de Kaenel (Chap. 16, this volume); and interpreted by Tandon et al. (1998) as a seismic discontinuity. Average sedimentation rates at this site are 400 m/m.y. for the lowermost cores just below the early Pliocene hiatus, 98 m/m.y. for the late–early Pliocene to late Pliocene, and 154 m/m.y. for the Pleistocene–Holocene (Shipboard Scientific Party, 1996c). Average sedimentation rates at Site 978 are 159 m/m.y. for the late Miocene, 120 m/m.y. for the early Pliocene, 111 m/m.y. for the late Pliocene, and 127 m/m.y. for the Pleistocene (Shipboard Scientific Party, 1996d).

According to the late Messinian age assigned to the 74 m of sediments underlying the gravel bed at Site 978 (Iaccarino and Bossio, Chap. 42, this volume), the probable age of this gravel is Pliocene or latest Messinian. Logging data, acquired only at Site 977 (quad-combo and FMS), provided excellent images of the gravel interval in the lower part of the hole (downhole from 531 mbsf), in which the core recovery was extremely low. No postcruise work on these logging data has been performed yet.

Age and Geochemistry of Volcanic Pebbles

Pebbles from the aforementioned gravel interval sampled at Sites 977 and 978 consist of a collection of mixed volcanic rocks, accompanied by minor metasedimentary (chert, dolomite) and metamorphic (quartzite, quartz-schist, schist) pebbles. Some of the volcanic clasts are coated by a calcareous sedimentary cement suggesting that the gravel was derived from a partly cemented sandy conglomerate. Volcanic lithotypes in the gravel clast encompass basalt, andesite, dacite, rhyolite, meta-basalt, meta-rhyolite, and meta-dacite.

Hoernle et al. (Chap. 27, this volume) have carried out the $^{40}Ar/^{39}Ar$ dating and the major- and trace-element geochemical analysis of the volcanic pebbles. The samples range from basalts to rhyolites, belonging to the tholeiitic, calc-alkaline, and shoshonitic series. Plagioclase phenocrysts from dacites yield an isochron age of 6.4 ± 0.3 m.y., and a mean apparent age of 6.1 ± 0.3 m.y. Sanidine phenocrysts from rhyolites give an apparent age of 9.25 ± 0.02 m.y. Amphibole phenocrysts from basalts yield apparent ages ranging from 8.8 ± 2.9 m.y. to 11.8 ± 1.6 m.y., with an isochron age of 9.95 ± 0.64 m.y. and a mean apparent age of 9.90 ± 0.40 m.y. Plagioclase phenocrysts from dacite give apparent ages from 11.1 ± 1.3 m.y. to 13.8 ± 0.3 m.y. Other plagioclase crystals from dacite indicate an apparent age of 12.1 ± 0.2 m.y. Pebble samples, ranging from basalt to rhyolite, are

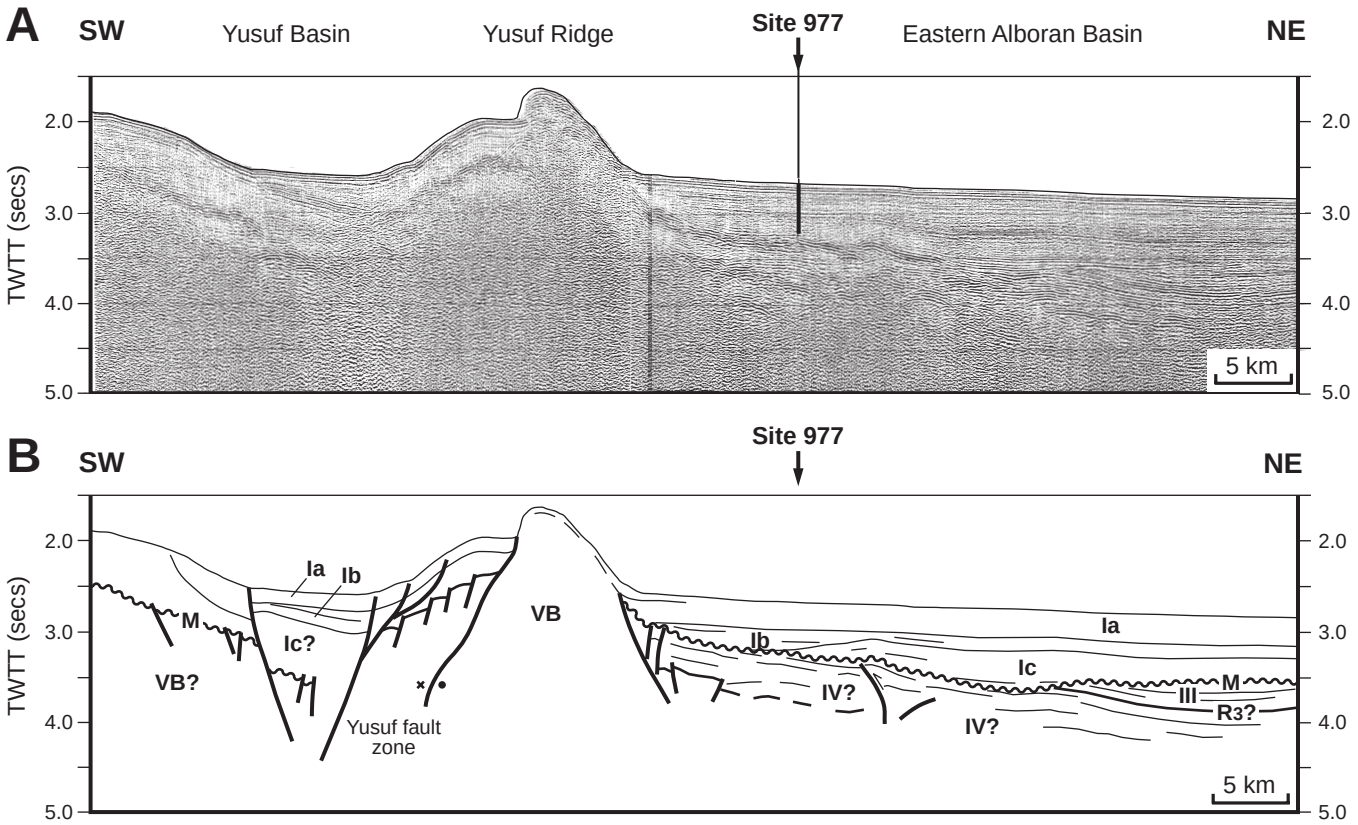

Figure 12. *JOIDES Resolution* seismic Line 3S (single channel) across Site 977. **A.** Original profile. **B.** Draw-line interpretation of Line 3S based on Site 977 data (modified from Alvarez-Marrón, Chap. 26, this volume). Reflectors and seismic units as in Figure 3. VB = Acoustic basement (volcanic rocks). Location of seismic line is shown in Figure 2. See explanation in the text.

attributed to tholeitic, calc-alkaline, high-K calc-alkaline, and shoshonitic series. Basalts and basaltic andesites have been divided into two groups on the basis of their rare-earth element (REE) pattern: (1) the LREE (lithophile and light REE) -depleted groups, with patterns similar to those observed in normal (N) and enriched (E) MORB (Mid-Oceanic Ridge Basalts), and (2) the LREE-enriched group, with patterns characteristic of OIB (Ocean-Island Basalts). The andesites, dacites, and rhyolites generally denote LREE-enrichment ($[La/Yb]_N \geq 1$), while the more evolved rock types have negative Eu anomalies, reflecting depletion of the MREE (medium REE). Among the basalt samples, the LREE-enriched basalts are characterized by a relative enrichment in Th and U and depletions in Rb, Ba, K, Zr, and Ti. In contrast, the LREE-depleted basalts show a relative enrichment in Rb, U, K, Pb, and Sr and a relative depletion in Th, Nb, and Ta. These basalt groups also display distinct immobile incompatible element ratios, with the LREE-enriched group having lower Ta/Nd, Sm/Nd, and Zr/Nb, but higher Ta/Yb, Th/Yb, Sm/Yb, Gd/Yb, and La/Nb than the LREE-depleted group.

According to Hoernle et al. (Chap. 27, this volume), fractionation of plagioclase, clinopyroxene, titanomagnetite, olivine, apatite, and amphibole can explain most of the observed variations in the major and compatible trace elements. On the basis of the presence of xenocrysts and the large range in Pb concentration in dacites and rhyolites (1.5 to 66 ppm, occasional samples having Pb of >15.5 ppm), they suggested that crustal contamination was an important process conditioning the chemistry of the most evolved magmas. Hoernle et al. (Chap. 27, this volume) conclude that the calc-alkaline affinities and the incompatible element systematics are characteristics of subduction zone volcanism, and that the immobile trace-element data indicate that the Miocene (6 to at least 12 Ma) asthenosphere beneath the Alboran region contained both depleted (MORB-type), peridotitic component and an ocean-island (OIB) or plume-type (HIMU) component, possibly in the form of garnet-pyroxenite layers.

Post-Miocene Contractive Structures

On the basis of the sediment ages constrained at Sites 977 and 978, seismic interpretation around the sites confirms that many bathymetric depressions and post-Messinian depocenters in the eastern Alboran Sea region are very recent wrench-related transtensional structures (Fig. 4). The M-reflector (base of the Pliocene–Pleistocene sequence, sampled at Sites 977 and 978) embodies a key reference for structural interpretations (Figs. 16–19 on back-pocket foldout, this volume).

JOIDES Resolution Line 3S (Fig. 12) and *Conrad* line 823 (Fig. 19 on back-pocket foldout, this volume) image the Yusuf right-lateral strike-slip fault system (Mauffret et al., 1987). The Yusuf Basin, containing sediments up to 2000 m thick, is bounded by the Yusuf Fault to the northeast. The Yusuf Fault, with an apparent vertical throw of >2 km, is interpreted as being the master-fault of the system. The rhomboid-shaped Yusuf Basin is a negative flower-structure (pull-apart-type, transtensive basin), and the adjacent Yusuf Ridge (900 m high) has been interpreted as a positive flower-structure (compressive feature) within the Yusuf strike-slip system (Alvarez-Marrón, Chap. 26, this volume).

Striking images appear in the northeastern half of Line 3S. The M-reflector (placed at the bottom of Hole 977A, Fig. 12) images a channeled erosional-surface cutting a faulted and slightly folded sedimen-

tary sequence of unknown age. Over the M-reflector, seismic Subunit Ic sampled at Site 977 (68 m thick interval, early Pliocene) seems to be part of a thicker-to-the-northeast lower Pliocene sequence in the East Alboran Basin. At the northeastern end of the seismic line, the lower Pliocene reflections represent ponding or onlapping sediments upon the erosional M-reflector surface; however, these reflections (Subunit Ic) show synsedimentary folding very near Site 977. Therefore, the reported brief hiatus within the lower Pliocene cores at Site 977 (Siesser and de Kaenel, Chap. 16, this volume) may be associated with contemporaneous uplifting of the antiform limb in Subunit Ic: the antiform seems to be related to the culmination of a steep reverse-fault in the underlying sediments. In the eastern flank of the Yusuf Ridge, the lower Pliocene sequence is missing, and the M-reflector and underlying reflections are uplifted and dragging up on the steep-faulted ridge flank. This uplifting does not involve the upper Pliocene (seismic Subunit Ib) or the Pleistocene sediments (seismic Subunit Ia). The main conclusion to be drawn from the seismic images and Site 977 results is that the fault that limits the Yusuf Ridge to the northeast was active before or during the early Pliocene, but not later on. The fault forming the southern scarpment of the Yusuf Ridge (the Yusuf Fault), however, was active till the Present, as demonstrated by the considerable uplifting of the Pleistocene–Holocene sequences near the top of the southwest flank of the ridge ("perched basins" in Fig. 19, back-pocket foldout, this volume).

A significant angular unconformity can be noted in the northern end of Line 3S, at a depth of about 3.5 s TWT, between the Pliocene–Pleistocene sequence and sediments (more than 1.7 s TWT thick) underlying the M-reflector (Fig. 12). Although no sample information exists here for sediments beneath the M-reflector, MCS seismic correlation in the region suggests that the high-reflectivity reflector at about 3.7 s TWT may be correlated with reflector-R3 (base of seismic Unit III, late Tortonian, Fig. 3). Hence, sediments below the gravel interval (M-reflector) sampled at Site 977 probably belong to seismic Unit IV, i.e., to the middle Miocene–early Tortonian sequence of the East Alboran Basin. Images from *Conrad* Line 823 (Fig. 19 on back-pocket foldout, this volume) confirm the presence of an unconformity below the Pliocene sequence sampled by drilling, and sediments up to 2 s TWT thick underlying the M-reflector.

Site 979 (South Alboran Basin)

Site 979 (Shipboard Scientific Party, 1996e) was drilled south of the Alboran Ridge in the northern South Alboran Basin (Fig. 2). The basin corresponds to a fault-bounded depocenter with variable sedimentary thickness, probably partially overlying, or interlayering, volcanic rocks similar to those forming the Alboran Ridge (Fig. 4; Figs. 17, 18 on back-pocket foldout, this volume). Site 979 sampled middle-to-upper Pliocene (NN16A to NN19A, seismic Subunit Ib) and Pleistocene/Holocene open-marine (seismic Subunit Ia), hemipelagic monotonous deposits to a total depth of 580.9 mbsf, where drilling had to stop to allow time for logging operations before the end of Leg 161 (Fig. 3). The Pliocene/Pleistocene (NN19A/NN 19B) boundary is at ~345 mbsf. Average sedimentation rates at Site 979 are comparable to the other sites (184-191 m/m.y., late Pliocene; 200 m/m.y., Pleistocene), but below a short hiatus within the late Pliocene (Siesser and de Kaenel, Chap. 16, this volume), biostratigraphic ages suggest a dramatic increase in sedimentation rate to 696 m/m.y. downsection.

Quad-combo logging data were acquired from 60.0 to 277 mbsf and the entire logged section confirms the homogeneity of the sampled sediments. Heat-flow estimation from thermal logging at Site 979 is 79 mW m^{-2}, in contrast to that reported by Polyak et al. (1996) in the South Alboran Basin, which reached average heat-flow values of 118 ± 8 mW m^{-2}. However, Shipboard Scientific Party (1996e) note that calculating heat flow using the shallowest measurement at 20.5 mbsf and its delta temperature (in situ minus mudline) of 2.04°C provides a heat-flow value of 111 mW m^{-2}, close to that reported from nearby sites. This suggests that there may have been a recent change in bottom-water temperature at the drilled site (Shipboard Scientific Party, 1996e).

Uplifting of the Alboran Ridge

Sedimentary strata are largely horizontal in the drilled section, with some cored dipping-bed intervals suggesting synsedimentary slumping within the recovered Pliocene–Pleistocene sequence. Nevertheless, seismic images across Site 979 (Figs. 17, 18 on back-pocket foldout, this volume) indicate a zone of Pleistocene-to-Holocene deformation (post-M-unconformity) and tilting imaged as a series of folds and faults extending from the southern flank of the Alboran Ridge to the adjacent basin floor. The lowermost sediments sampled at Site 979 (middle Pliocene) lie a few dozen meters above a major angular unconformity, seismically correlated to the M-unconformity (equivalent to the gravel interval) cored at Sites 977 and 978 (Shipboard Scientific Party, 1996e). Line *Conrad* 825 (Fig. 17 on back-pocket foldout, this volume) clearly evidences the existence of post-Messinian compressional structures in the Alboran Basin. At the southern flank of the Ridge, the attitude of the Pliocene-to-Holocene syntectonic sediments suggests that folds developed above a near-vertical reverse fault, and the northern flank of the Ridge shows comparable fault-related uplifting of syntectonic Pliocene to Holocene sediments, but folding is absent. The volcanic Alboran Ridge represents a positive, antiformal flower-structure related to a left-lateral strike-slip system that extends along more than 120 km to the Xauen Bank (comprising folded sediments), and aligns with the Jebha Fault (Fig. 4; Figs. 16–18 on back-pocket foldout, this volume).

Seismic images (Fig. 17 on back-pocket foldout, this volume) and the age of sediments at Site 979 confirms that later uplifting of the Alboran Ridge occurred from the late Pliocene to the Holocene. The high sedimentation rate at this site indicates that uplifting was coeval with active subsidence. No significant volcanic or volcaniclastic material was sampled at Site 979, evidencing that late Pliocene-to-Pleistocene uplift of the Ridge was not accompanied by nearby volcanic activity. This implies that volcanism at the Alboran Ridge was not active at these times.

VALIDATING DRILLING RESULTS ON THE ORIGIN AND TECTONIC EVOLUTION OF THE ALBORAN BASIN

In this section we focus on an overview of the relevance of scientific results from Leg 161 with regard to the geological and geophysical background of the Alboran region, and also on the major questions left incompletely resolved by drilling in the Alboran Basin. In our opinion, one of the main contributions of Leg 161 derives from the results at Site 976 because those results have provided essential clues about the origin of the basin. Nonetheless, drilling results in the East and South Alboran Basins (Sites 977, 978, and 979) helped to better constrain the timing of later tectonic stages in basin evolution and, therefore, to discern the reasons for the present structural pattern in the westernmost Mediterranean region (Figs. 13, 14). New findings revealed by drilling improve current knowledge on the tectonic evolution of the basin (Fig. 15).

The two crustal sections in Figure 14 illustrate east-west (Fig. 14A) and north-south (Fig. 14B) true-scale structures across the Alboran Basin itself and the peripheral arcuate thrust-belt in the Gibraltar region and Betic and Rif Chains. These sections accommodate shallow structures shown in the map in Figure 13, and illustrate the areal distribution and organization of the distinct crustal domains, as well as the abrupt crustal thinning that characterizes the transition from the Betics and Rif to the Alboran Sea. The subcrustal structure for the

whole region is quite debatable, as available geophysical data are not sufficient to confidently depict the lithospheric structure yet.

Effective constraints of extension-related exhumation history at Site 976 are given by the cooling history of the basement (Hurford et al., Chap. 21, this volume; Platt and Kelley, Chap. 22, this volume; Platt et al., in press). As detailed in the previous sections, thermal modeling of the P-T path indicates that exhumation of the basement, occurred very rapidly, at an average rate of more than 4 km/m.y. Because the required total time for exhumation of metamorphic rocks from 40 km depth to the surface is about 9 m.y., Platt et al. (in press) propose that the extensional denudation and thinning of the Alboran Crustal Domain started during the late Oligocene (at about 27 Ma); in other words, somewhat before the marine transgression that created the Alboran Sea (Fig. 15). Results from drilling therefore support previous suggestions, based on analysis of the subsidence history, that part of the crustal thinning in the Alboran Domain occurred above sea level (Watts et al., 1993).

It is worth remarking that the P-T path of the high-grade schist at Site 976 contrasts with the published P-T paths of the different units in the Alpujárride Complex of the Alboran Domain in the western Betic Cordillera, particularly with regard to the occurrence of an increase in temperature during the extensional decompression path (Fig. 11). The current P-T evolution of these Alpujárride Complex units considers a conspicuous pressure drop (with an estimated -ΔP >10 kbar) under isothermal conditions (e.g., García-Casco and Torres-Roldán, 1996; Balanyá et al., 1997; Azañón et al., 1998). After the decompression, the different Alpujárride units show quick cooling histories (100°–350°C/m.y.; Zeck et al., 1992; Monié et al., 1994), comparable to that at Site 976.

The lithologic association at Site 976 broadly resembles some that are found within the Alpujárride Complex. Sánchez-Gómez et al. (Chap. 23, this volume) suggest that rocks sampled at Site 976 correlate with a specific Alpujárride unit—the Ojén Unit—underlying the Ronda-peridotite slab in the western Betic Cordillera (30 km west-southwest of Málaga; Fig. 4). Like the basement samples at Site 976, this unit is formed of marbles, high-grade schist, amphibolite, and gneiss, with abundant migmatite and leucogranitic rocks (granite and granodiorite). Leucogranite occurs as late dikes cutting most of the ductile structures and as large sheet-like bodies associated with a shear zone that comprises the lower peridotite boundary (Sánchez-Gómez et al., Chap. 23, this volume). The P-T path presented for the Ojén Unit (Fig. 11B) shows a significant decompression path, from HP-conditions recorded in relict eclogite (P > 15 kbar at T = 720°–790°C; Tubía and Gil Ibarguchi, 1991) to low-P conditions (P ≈ 3–4 kbar at T = 650°–700°C) occurring at the end of the development of the main foliation (Sp) (Westerhof, 1977; Tubía et al., 1997; Sánchez-Gómez et al., Chap. 23, this volume). Furthermore, leucogranitic rocks formed at low-P conditions (5.5–4.2 kbar at 650°–680°C) during the latest stages of decompression and the initiation of the cooling path (Fig. 11). Therefore, in contrast with Site 976, the

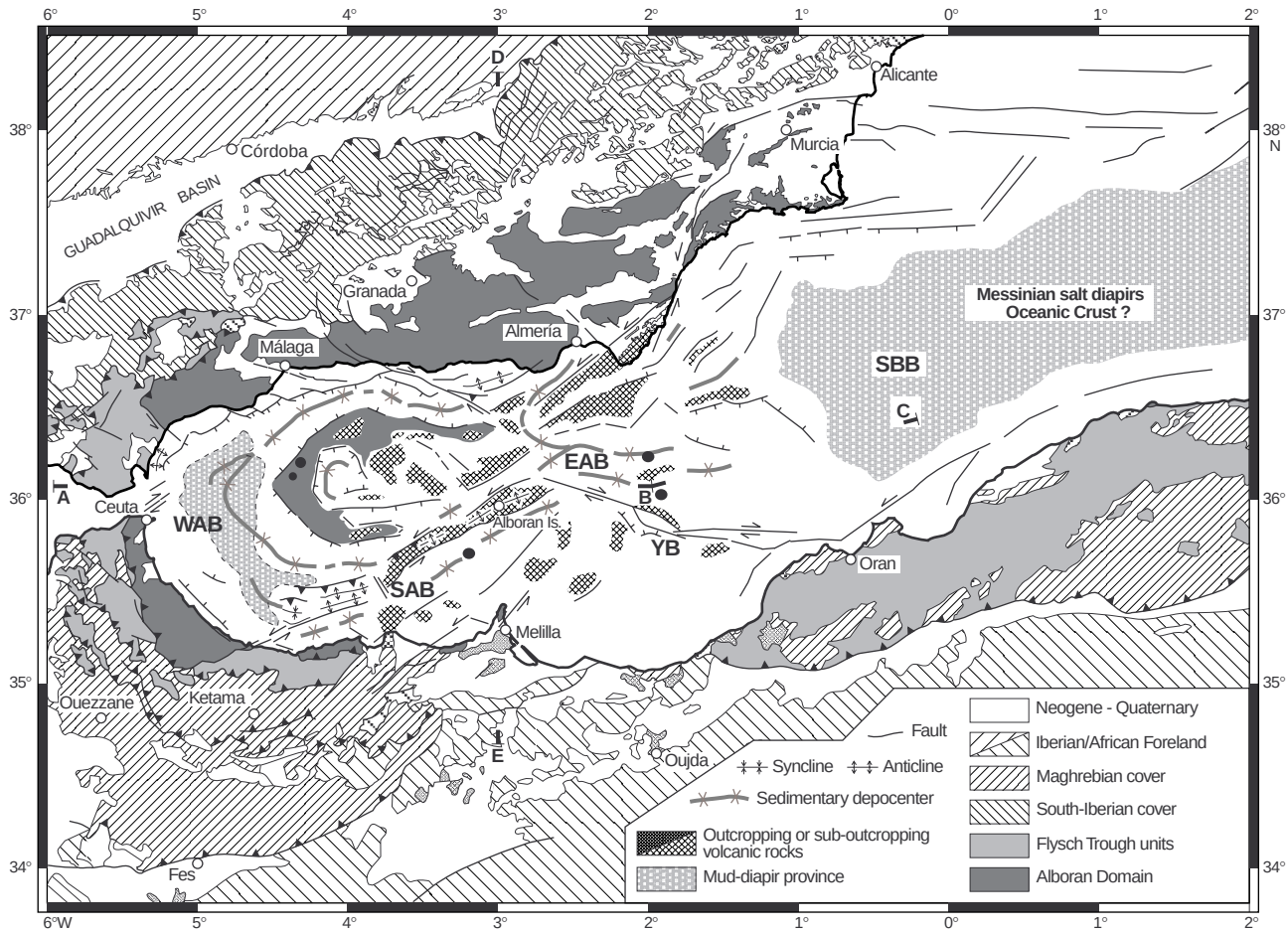

Figure 13. Tectonic map of the westernmost Mediterranean (Alboran and South Balearic seas). Note that the limits of the Messinian salt diapirs in the South Balearic Basin seem to fit with the inferred anomalous continental or oceanic crust as shown in Figure 14A. A, B, C mark the position of cross-sections in Figure 14. Black circles show location of Leg 161 sites and ODP Site 121 as in Figure 4.

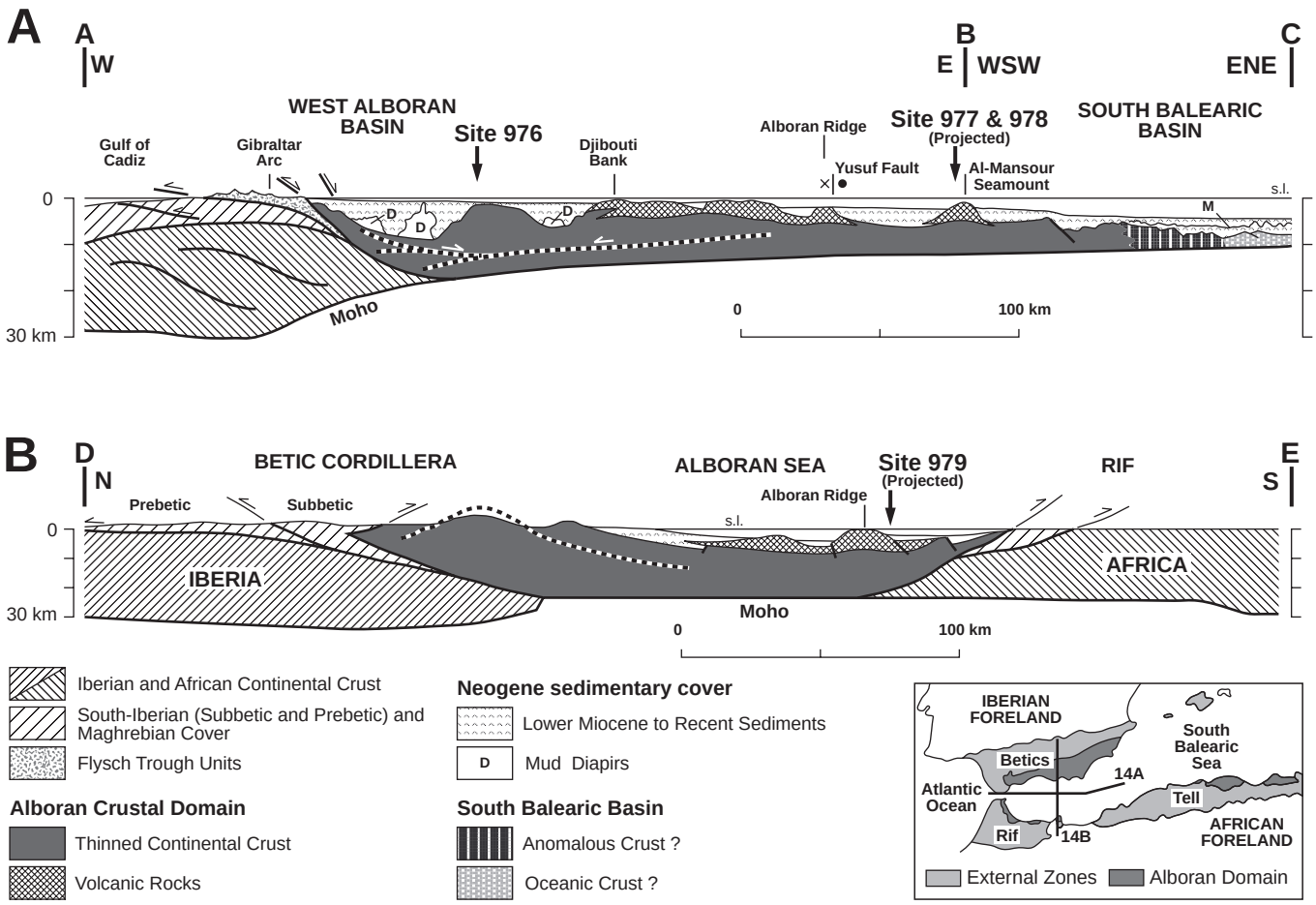

Figure 14. **A.** Schematic true-scale section from the Gibraltar Arc to the South Balearic basin to illustrate the east-west crustal structure of the westernmost Mediterranean (modified from Comas et al., 1993; Comas, Zahn, Klaus, et al., 1996), based on a synthesis of structural data from the Gibraltar region and MCS profiles in the Alboran Sea, 3D modeling, gravity consideration, surface heat-flow, and elevation data (Torné et al., unpubl. data). The modeled crustal thickness beneath the Alboran Sea is in agreement with available seismically derived estimates of the Moho depth. **B.** Schematic true-scale section to illustrate the north-south crustal structure of the Alboran Basin, based on a synthesis of structural data from Spain and Morocco and *Conrad* seismic lines and on a density model obtained by comparing observed and calculated Bouguer anomaly data (Watts et al., 1993). Note that both crustal sections confirm the thinning of the continental crust beneath the Alboran Basin, but modeling different data resulted in discrepancies on crustal-thinning values. A more conclusive estimate of crustal thickness variations deserves additional refraction and wide-angle reflection seismic data. The intracrustal reflectors (hatched white lines in the Alboran Domain), shown by the MCS *Conrad* profiles (Figs. 16–19 on back-pocket foldout, this volume), are interpreted as extensional detachment faults or the top of the reflective lower crust.

metamorphic evolution of the Ojén Unit does not record an increase in temperature during decompression.

The discrepancies in the metamorphic history make the correlation of the basement rocks at the Site 976 High and the Ojén Unit somewhat unclear, because lithologic similarities among the Alpujárride units, even if clear, should not be the only criteria for correlation. Further attempts at offshore-onshore basement correlation should consider that the low-P metamorphism and associated heating at Site 976 could be a particular feature of the basement beneath the Alboran Sea, where the crust is extremely thin. Identical metamorphic evolution would therefore not have occurred in other regions of the Alboran Domain where the crust is thicker (Fig. 14).

The crustal section in Figure 14A is based on a synthesis of structural data from the Gibraltar region and MCS profiles in the Alboran Sea, and 3D modeling, considering gravity, surface heat-flow, and elevation data (Torné et al., unpubl. data). The crustal thickness beneath the Alboran Sea estimated from this modeling is, for the most part, in agreement with available seismically derived estimates of the Moho depth. Seismic and modeled data suggest that the continental crust is about 18 km thick in the West Alboran Basin, thinning eastward to the East Alboran Basin (to less than 12 km), progressively giving way toward the east to an anomalous crust, with extensive volcanism, and then to a probable oceanic crust (basement of 2 s TWT in thickness) in the western South Balearic Basin. The eastern end of the crustal section in Fig. 14A is based on profile ESCI-Alb2, where isolated deep reflections distinguished between 6.5 and 7 s TWT underneath the Messinian salt diapirs have been interpreted as associated with the reflective Moho (Comas et al., 1997). The crustal section in Figure 14B is based on a synthesis of structural data from Spain and Morocco, on *Conrad* seismic lines, and on a density model obtained by comparing observed and calculated Bouguer anomaly data (Watts et al., 1993). The density model proposes a thicker crust (up to 22 km; Fig. 14B) beneath the Alboran Sea than that obtained from the 3D model (up to18 km, Fig. 14A). A possible reason for the discrepancy in the modeled crustal-thickness values could be that the 3D model (which gives a lower crustal thickness) considers the gravity effect of the asthenospheric mantle, deduced from the heat-flow density values in the region. The lack of refraction and wide-angle reflec-

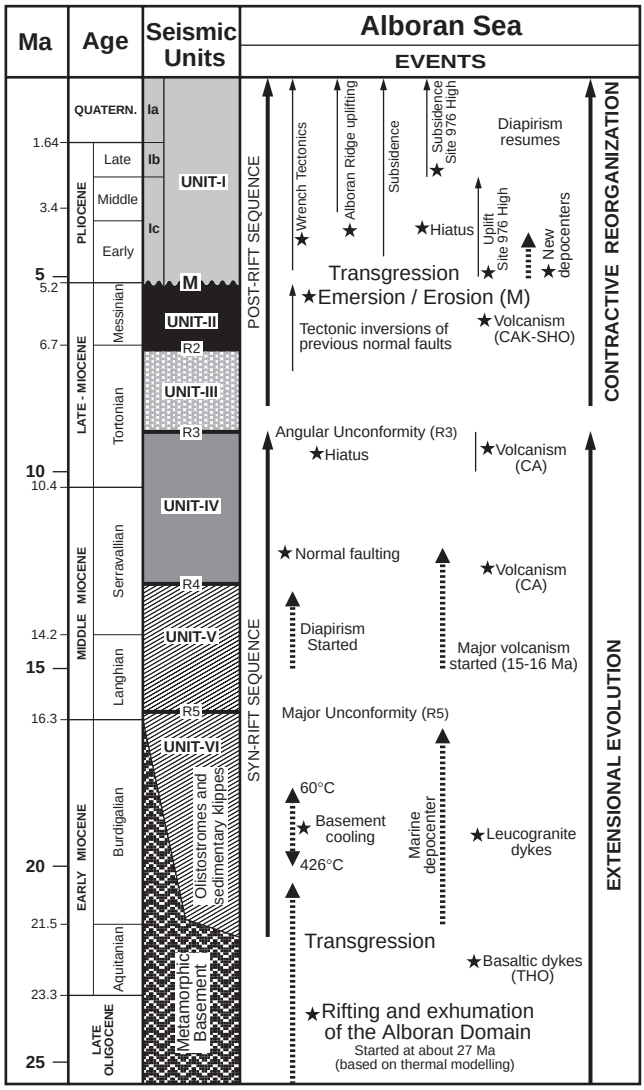

Figure 15. Timing of main events in the tectonic evolution of Alboran Basin constrained by Leg 161 results (marked by stars) and other data considered in this synthesis. All events annotated here are commented upon in the text.

tion seismic data, for example, makes it difficult to present a conclusive value for the crustal thickness in the region; although both crustal sections confirm that the continental crust beneath the Alboran Basin has been substantially thinned. Further geophysical constraints are needed to determine the true amount of crustal thinning.

Much of the crustal stretching during the Miocene rifting can be related to intracrustal low-angle extensional detachments seen in the deep MCS reflection profiles, implying these detachments drove and accommodated the shallow extensional structures observed in the Alboran Basin (Fig. 14). Intracrustal reflectors (ICR; Figs. 16, 18 on back-pocket foldout, this volume), interpreted as probable extensional shear-zones (mylonitic zones), are imaged in the *Conrad* lines between 4 and 7 s TWT in the northern Alboran Sea margin, with an apparent dip to the south (Watts et al., 1993). In the ESCI-Alboran 1 line, located at 3ºW meridian in the Spanish shelf and striking N20ºE across the northern Alboran Sea, similar ICR can be seen, with an apparent dip to the south-southwest, between 6 and 8 s TWT in depth (Comas et al., 1997). The ICR observed in ESCI-Alboran 1 line, probably represent the continuation of a near-flat prominent reflective band, recognized at about 6 s depth in the ESCI-Béticas 2 line (striking N30ºE across the Alboran Domain near the coastline at 3ºW meridian), also interpreted as an extensional shear-zone or a mid-crustal decoupling level (García-Dueñas et al., 1994; Martínez-Martínez et al., 1997b). Reflectors interpreted at the top of the reflective lower crust (TLRC; Figs. 16, 18 on back-pocket foldout, this volume), imaged at about 6–8 s TWT in depth in the *Conrad* lines (Watts et al., 1993), can also be observed as a band of highly coherent reflectivity between 6-9 s TWT in depth in the ESCI-Alboran 1 line (Comas et al., 1997). The bottom of this beam of reflections (TLRC) might be attributed to the Moho boundary discontinuity, which is in agreement with results from stacked wide-angle data in the ESCI-Betics 2 line (Carbonell et al., 1997). Intracrustal seismic images, and consistency between the timing of extensional episodes reported from offshore and onshore regions, suggest that the crustal thinning beneath the northern Alboran Sea basin is linked to the extensional detachment-systems in the Betic Chain.

Drilling data demonstrated that the Site 976 High was exposed to the seafloor by the late Serravallian, but near-site MCS profiles (Figs. 16, 17 on back-pocket foldout, this volume) suggest that the basement high has been submarine, or occasionally emergent, relief since the early Miocene. Major unconformities within the early to middle Miocene sedimentary cover (reflectors R5 and R4; Figs. 8, 15) are probably a result of pulses of fault activity during the rifting processes. The R3 reflector (Figs. 3 and 8), appears to mark the end of Miocene rifting in the Alboran Basin (Fig. 15). On the whole, seismic interpretations support the existence of low-angle, fault-related continuous extension in the basin from the Aquitanian?-Burdigalian (the age of the marine transgression) to the early–late Miocene (Fig. 15), in agreement with subsidence data from the Andalucía-A1 well (Fig. 6). Different directions of local Miocene extension (south-southeast, southwest, west-southwest, and northeast) have been reported in the Alboran Basin; nonetheless, a resulting direction, with the top to the southwest or south-southwest, of maximum extension appears to dominate the Miocene rifting (Fig. 4). Changes in direction of extension are probably caused by the interplay of transfer-faults within the middle-to-late Miocene extensional system, which may in turn have been conditioned by previous early Miocene extensional faults.

Drilling results also provided information of certain events of the postrift contractive deformation of the Alboran Basin (Fig. 15). Directions of compression are indicated by east-northeast–west-southwest trending folds and sinistral northeast-southwest and north-northeast–south-southwest, and dextral west-northwest–east-southeast strike-slip conjugate fault systems (120°–130° angles between the two strands; Fig. 13). The contractional deformation was dominated by post-Messinian wrench tectonics (Figs. 16–19 on back-pocket foldout, this volume); the conjugate strike-slip faults give way to both transtensive conditions that originated new depocenters (e.g., the Alboran Trough and the Yusuf Basin) and a transpressive situation producing local uplifting (positive flower-structures) by oblique-reverse strike-slip faults and folds (e.g., the Alboran Ridge and its prolongation at Xauen Bank). Most of these faults are active presently, leading to distributed seismicity in the region. The focal mechanisms of earthquakes and moderate teleseisms document the present-day state of stress in the basin, which is quite variable from one site to another, in accordance with the distinct types of deformation now occurring in the region (Morel and Meghraoui, 1996; Calvet et al., 1997; Mezcua and Rueda, 1997). De Larouzière et al. Chap. 24, (this volume) confirm a predominant southwest-northeast extensional (or transtensional) present-day situation at Site 976, in agreement with positive subsidence in the West Alboran Basin since the late Pliocene (Fig. 6). Significant morphological lineaments in the Alboran Sea basin and in its transition to the South Balearic Basin (e.g., the Palomares and Carboneras strike-slip shear zones, Figs. 4 and 13; Weijermars, 1987; Keller et al., 1995) formed as a result of this compression. Contractional structures are congruent with those known in areas surrounding the Alboran Sea (de Larouzière et al., 1988; Mon-

tenat, 1990). The post-Messinian deformation of the basin is consistent with the north-northwest/north current convergence of Iberia and Africa.

Subsidence analysis at the Site 976 High and commercial wells provide new data on the subsidence/uplift history of the marine basin (Fig. 6; Rodríguez-Fernández et al., Chap. 5, this volume). Subsidence data at this site reveal significant events in basin evolution: rapid tectonic subsidence (at rates of 3 km/m.y.) from the late Serravallian till the early Tortonian, gentle subsidence till the earliest Pliocene, relative uplift of the structural high during the early Pliocene, and an active subsidence-pulse by the earliest Pleistocene. New data from the Andalucía-A1 well denote three episodes of rift-related subsidence at 15.5–14.5 Ma (Langhian-early Serravallian), at 13–10.7 Ma (late Serravallian), and at 9.2–8.5 Ma (Tortonian), separated by episodes of uplifting. These results are somewhat different from previous subsidence estimates in the Andalucía-A1 well (Watts et al., 1993; Docherty and Banda, 1992, 1995), probably because the backstripping technique used to obtain the subsidence trend presented here first includes paleobathymetric corrections. Subsidence analyses across the Alboran Basin indicate a conspicuous lateral variation of rift-related subsidence phases, suggesting migration of locus of extension, and probably also changes in extensional-transport direction during Miocene rifting. Differences of subsidence amount and rate during contemporaneous rifting-phases were probably related to different basement tilting or rotation. Early Pliocene uplift and earliest Pleistocene (at about 1.7 Ma) rapid subsidence at Site 976 could represent tectonic events during the post-Messinian contractive reorganization of the basin; the rapid subsidence probably being related to episodic transtensional conditions in the West Alboran Basin. The almost general gentle phase of subsidence that affected the entire basin during post-Messinian times, contemporaneous to its contractive reorganization, has been interpreted either as thermal (Watts et al., 1993) or as flexural subsidence (Docherty and Banda, 1995). From the latest Tortonian onward, the overall negative trend of the subsidence in the onshore Neogene Basins (e.g., Granada Basin, Fig. 6) indicates general uplift at the basin margins, in agreement with the changeover from marine to continental deposits since the early Pliocene in these intramontane basins (Sanz de Galdeano and Vera, 1992).

Although Leg 161 did not drill or sample any in-situ volcanic rocks, geochemical studies, and Ar/Ar age-dating of reworked volcanic pebbles recovered at shallow sedimentary levels in the Eastern Alboran Basin yield additional information on the characteristics and ages of the middle and late Miocene magmatism in the region (Fig. 15). The Neogene volcanism in the Alboran Sea is better developed in its central and eastern parts, thus suggesting more vigorous magma production on this side of the basin (Fig. 13). In southern Spain, volcanic rocks lie within the Neogene Betic basins and also in the Alboran Domain of the Betic Chain, with a few located in the Betic External Zones. Magmatic rocks in the central-western Betics include basic dikes of tholeiitic affinity of about 23-22 Ma (K/Ar dating; Torres-Roldán et al., 1986) and leucogranites at about 18–20 Ma (Ar/Ar dating; Zeck et al., 1989, 1992; Monié et al., 1994). Magmatic products in the Cabo de Gata region, the most ample volcanic province (about 400 km^2) in the Betic Chain (Figs. 4 and 13), belong to calc-alkaline series containing all the petrological types, from basic to acid volcanism (e.g., Fernández-Soler, 1992; 1996). In the Almería and Murcia region, scattered shows of magmatic rocks belong to a peraluminous (S-type) volcanic province and to an ultrapotassic (lamproitic) suite, giving way to the northeast to Pliocene alkaline basalts in the area of Cartagena. In the Rif, magmatic manifestations include calc-alkaline andesitic and rhyolitic suites, as well as shoshonitic and alkaline-sodic suites of late Miocene and Pliocene age; similar rocks appear farther east in the Oran area (Araña and Vegas, 1974; Bellon et al., 1983; de Larouzière, 1985; Hernandez et al., 1987; Louni-Hacini et al., 1995). Ages (mostly K/Ar dating) of typical calc-alkaline series in the eastern Betics and Rif range from 15 Ma to 8 Ma, the shoshonitic to lamproitic lavas occurred at about 9-4 Ma, and the alkaline basalts erupted from 6 to 1.7 Ma (Bellon et al., 1983; Hernandez and Bellon, 1985; Di Battistini et al.,1987; Hernandez et al., 1987).

In the marine realm, the Alborán Island is formed of low-K basalts and andesites and reported radiometric-age data are imprecise and quite discordant (9-9.2 Ma, Hernandez et al., 1987; or 7 Ma and 18 Ma, Aparicio et al., 1991). Volcanic rocks from Alboran seafloor scarpments have been obtained recently by diving with the submersible *Cyana* on the northern flank of Alborán Island, at the Yusuf Fault scarpment, and at Al-Mansour Seamount (Fig. 4). Samples recovered by diving are mainly composed of rocks of calc-alkaline rhyolite and low K-basalt to andesite series, yielding K/Ar radiometric ages of 10.1 ± 0.8 Ma (andesite, from the whole rock) and 9.6 ± 0.3 Ma (rhyolite, from biotite) in the Yusuf scarpment and the Alborán Island, respectively (Fernández-Soler and Comas, unpubl. data).

The Ar/Ar age dating in the volcanic pebbles from both Sites 977 and 978 presented by Hoernle et al. (Chap. 27, this volume) register the magmatic activity to a time span of about 6 m.y. (from 12 Ma, Serravallian, to 6 Ma, Messinian). The authors emphasize that the volcanic pebbles are older in age downcore at Site 978; therefore, they suggest the volcanic clasts to have been deposited shortly after their eruption. However, this conclusion is not consistent with drilling data, which indicates that cored pebbles, being thinner in diameter than the core liner (maximum diameter of volcanic pebbles is ~6 cm, minimum ~1 cm), are mixed when logged along the core liner. Biostratigraphic ages recorded in fine-grained marine facies overlying and underlying the gravel interval at Site 978 (Iaccarino and Bossio, Chap. 42, this volume; de Kaenel and Siesser, Chap. 16, this volume) imply that volcanic pebbles are reworked, mixed with sedimentary and metamorphic clasts, and deposited all together in a sedimentary gravel bed by the latest Messinian or shortly afterward (i.e., after 5.6 Ma). Hoernle et al. (Chap. 27, this volume) also declare that the volcanic pebbles proceed from volcanic areas adjacent to the drilling sites, which would not be entirely plausible. As pointed out by the Shipboard Scientific Party (1996c, 1996d), because the gravel interval has been found at similar stratigraphic positions—corresponding exactly to the M-reflector—at sites located 37 km apart, the gravel beds likely occupy latest-Messinian or lowermost-Pliocene submarine paleo-valleys; the volcanic pebbles could therefore mainly correspond to detritus from the Almería and Cabo de Gata region that moved out toward the South Balearic Basin along the valley bottoms.

Models and Possible Causes of Extension in the Alboran Sea

The hypotheses currently most widely debated to explain the formation of the Alboran Sea basin can be summarized as follows:

1. Extension was related to forces transmitted from a convergent plate boundary associated with the External Betic-Rif thrust belt. In their simplest form, these forces are thought to arise from the "rollback" of a subduction zone beneath the Alboran region (de Jong, 1991; Zeck et al, 1992; Royden, 1993; Zeck, 1996; Lonergan and White, 1997). The subduction zone, when supposed to lie to the west of the Alboran Domain, is thought to have retreated westward during the course of the Miocene from somewhere within the western Mediterranean, either to the present position of the Gibraltar Arc (e.g., Lonergan and White, 1997) or to the Horseshoe Seamounts in the eastern Atlantic (e.g., Royden, 1993).
2. Extension was a result of delamination of the lithospheric mantle from beneath the crust of the Alboran Domain (García-Dueñas et al., 1992; Comas et al. 1993; Docherty and Banda, 1995; Seber et al., 1996). This concept is based on the suggestion by Channell and Mareschal (1989) that coeval extension

and compression in the Tyrrhenian Sea and the associated Calabrian arc could be a result of asymmetric detachment and removal of the lithospheric mantle.

3. Extension was a consequence of the convective removal of the lower part of the conductive thermal boundary layer beneath a region of thickened crust and lithosphere produced by pre-Miocene convergence between Africa and Iberia (Platt and Vissers, 1989). The latter hypothesis drew on suggestions that the change from a compressional to an extensional tectonic regime in other areas of active continental collision, such as Tibet, is a result of the convective removal of the lower part of the thickened lithosphere beneath the orogen (England and Houseman, 1989).

The principal tectonic objective of ODP Leg 161 was to obtain information that could constrain these and other models for the origin of the Alboran Sea. All three models summarized above are based on ideas and assumptions about the mechanical behavior of the lithosphere in convergent plate settings and are difficult to test directly. It is therefore appropriate to consider what predictions these models make that could be tested by near-surface observations. The most obvious differences among them are in the predictions they make about (a) the thermal structure of the lithosphere and (b) the history of surface elevation; and (c) the nature and distribution of the magmatism.

The rollback model attributes extension primarily to forces applied at a distance. Extension is therefore "passive" in that convective or advective motion of material and heat is not the primary cause of lithospheric deformation. The thermal structure of the lithosphere during extension should therefore be simply predictable as a result of horizontal stretching. This causes the thermal gradient to increase, but individual material points within the lithospheric column will either decompress isothermally (if extension is rapid compared to the characteristic time for conductive cooling to the surface) or they will cool (Ruppel et al., 1988), unless there is significant heat input from crustal radioactivity or from magmatism. The upper surface of the lithosphere should on average subside throughout this process (McKenzie, 1978) as a result of crustal thinning, cooling of the stretched lithosphere, and sediment loading. Local uplift may occur in the footwalls of major faults during rifting. Furthermore, contemporaneous magmatism is predicted to have a subduction component signature. Passive extension is unlikely to be associated with significant magmatism unless the mantle potential temperature is abnormally high, or the amount of extension is very large (McKenzie and Bickle, 1988). Any contemporaneous magmatism is therefore likely to be related to subduction at the plate boundary and should show an appropriate geochemical signature.

Delamination, as originally proposed by Bird (1978), on the other hand, involves the wholesale removal of the lithospheric mantle, bringing asthenospheric material to the base of the crust. This would cause a dramatic step in the geotherm, which would decay, producing substantial temporary heating of the crust. This heating may accompany decompression during extension, producing distinctive P-T paths. Substantial melting of the lower part of the crust may occur as a result of this heating, depending on its precise composition, and melting would be further stimulated by the rise of basaltic magma produced by decompression melting in the underlying asthenosphere. At the same time, the removal of the negatively buoyant mantle lithosphere could result in as much as 3000 m of surface uplift, depending on the initial thickness and composition of the lithosphere. This would then be followed by rift-related subsidence as extension gets under way, and then by thermal subsidence. Both types of subsidence should proceed at a higher rate initially than in the case of passive rifting because of the absence of the negatively buoyant and thermally insulating mantle lithosphere, but the total subsidence, once the lithosphere has reached full thermal equilibrium, would eventually be the same for a given amount of extension.

The concept of convective removal of the lower part of a lithospheric root as the driving force for extension in orogenic settings lies somewhere between the two other hypotheses in terms of its implications for the thermal evolution and subsidence history. Removal of part of the lithosphere should cause a step in the geotherm, and hence some degree of heating of the overlying crust and the remaining lithospheric mantle (Platt and England, 1994), partial melting within the lithosphere, and also some initial uplift (possibly 2-3 km; England and Houseman, 1989). The amounts of heating and uplift would be less than in the case of complete delamination, depending on how much of the lithosphere is removed.

It follows from the above that both the thermal evolution of the extended crust, the magmatism, and the uplift and subsidence history of the region should contain information constraining these hypotheses. The seismic and drill-hole information obtained during Leg 161 should therefore make a significant contribution toward resolving this question for the Alboran Sea.

The character of the Alboran Basin magmatism is an important factor discerning among competing models for basin formation; however, proposed magmagenetic models for the calc-alkaline rocks of the Alboran Domain remain controversial. Magma generation has been related to the melting of one (e.g., Araña and Vegas, 1974) or two (e.g.,Torres-Roldán et al., 1986) subducted oceanic crusts, in an early Miocene subduction; to melting of an ancient subducting, rolled-back or detached, lithosphere slab (e.g., de Jong, 1991; Zeck, 1996; Lonergan and White, 1997); associated with a trans-Alboran crustal shear zone (de Larouzière et al., 1988); or related to lithosphere mantle removal or delamination (Fernández-Soler, 1992, 1997).

Hoernle et al. (Chap. 27, this volume) affirm that the calc-alkaline affinities and the incompatible element systematics in volcanic pebbles from Sites 977 and 978 are characteristic of subduction-zone volcanism, indicating that their geochemical signature, and certain geophysical evidences, support a northwest-dipping oceanic-subduction zone beneath the eastern Alboran from 6 to at least 12 Ma; in addition, these authors propose that a Pliocene "slab detachment and lithosphere delamination" followed the late Miocene subduction. However, given that many subduction-related magmas obtain their geochemical signature by the addition of subducted sediment to shallow mantle-derived melts (e.g., Tatsumi and Eggins, 1995), the use of geochemistry may be problematic in distinguishing them from crustally contaminated asthenospheric melts (Kay and Kay, 1993).

Geochemical work on the very similar suites of volcanic rocks exposed onshore in the eastern Betic Cordillera, however, suggest that alternative interpretations of the geochemistry are possible (S. Turner, pers. comm., 1998). A calc-alkaline suite exposed in the Cabo de Gata region, with an age range comparable to the pebbles found at Sites 977 and 978, show enrichment of the more incompatible trace-elements, such as Rb, Th, and U, and are markedly LREE-enriched with a variable negative Eu anomaly. They have prominent negative Ba, Ta-Nb, and Ti anomalies and a large positive Pb anomaly, relative to primitive mantle. Modeling of trace-element ratio–isotope arrays indicates that these magmas can be interpreted as representing variable degrees of crustal contamination (20%–50%) of MORB-type melts produced by shallow melting within asthenospheric mantle. Similar conclusions have been reported from extensive geochemical data (trace-element/isotopic modeling) carried out in numerous rock-types and wide age spectrum of the calc-alkaline and shoshonitic volcanism in the Cabo de Gata region (Fernández Soler, 1992, 1996). The geochemical characteristics of the Alboran-Yusuf low-K mafic suite sampled by diving suggest that these rocks are less evolved than the Cabo de Gata calk-alkaline series, probably because of the very thinned crust in this marine region. Incompatible/immobile element data from these rocks indicate a depleted MORB source area (flat to LREE-depleted patterns), and the presence of an "arc component" signature (lithophile [LIL] element enrichment, relative

depletion of Nb and Ta). Their $^{87}Sr/^{86}Sr$ contents are higher than typical mantle values and much higher than depleted mantle values, thus indicating the presence of a metasomatizing sialic (crustal) components in the magmas. Modeling of trace-element ratio–isotope arrays also suggests that these magmas could derive from a depleted mantle source, to which the "crustal" or "slab" component has been introduced from partial melting of both crust and heterogeneous mantle by upwelling of hot asthenospheric mantle (Fernández-Soler and Comas, unpubl. data).

It is worth noting that all three hypotheses discussed here are subject to variations in terms of the geometry and kinematics of the process, so that observations on the geometry and kinematics of extension in the basin may not be definitive in distinguishing among them. An example of this is that two recent proponents of the trench rollback hypothesis (Royden, 1993; Lonergan and White, 1997) suggest quite different end positions for the subduction zone. Similarly, recent advocates of mantle delamination have proposed that propagation in different directions (García-Dueñas et al., 1992; Docherty and Banda, 1995; Shipboard Scientific Party 1996a [Fig. 3]; Seber et al., 1996). The concept of convective removal of mantle can be similarly modified by the introduction of an arbitrary velocity for the extending Alboran Domain relative to the African and Iberian plates (e.g., Platzman, 1992).

The main conclusion of the thermal calculations from the basement at Site 976 is that, in the absence of evidence for substantial magmatic heat input, the substantial heating (by about 75°C) of the high-grade schist during decompression to very low pressures can only be explained by the removal of the mantle lithosphere below about 60 km. Removal of lithosphere at depths significantly greater than 62.5 km cannot explain the combination of high temperatures reached by the Site 976 high-grade schist and the shallow depth at which they attained maximum temperature. Given that this corresponds approximately to the thickness of the pre-extensional orogenic crust in the region, this is equivalent to delamination in the sense of Bird (1978).

Tectonic models for the formation of the Alboran Sea basin that involve lithospheric stretching in response to plate-boundary forces, without any removal of lithosphere, nor partial convective removal of the mantle lithosphere, cannot explain the late onset of heating and the high temperatures reached by Site 976 basement cores. It can be argued that one possible heat source to account for the observed increase in temperature during the latest Oligocene(?)–early Miocene exhumation of the Alboran Sea basement could be provided by contemporaneous magmatic activity. As stated above, in the western Betic Chain, the intrusive rocks are of early Miocene age (18–20 Ma for the leucogranite dikes and 22–23 Ma for the basaltic dikes) and have a limited extension. Volcanism is particularly important east of the 3°W meridian (Fig. 13), but it is younger in age (mainly developed from 15 Ma onward [Fig. 15]). In consequence, the magmatic activity in the Alboran Sea appears to have occurred after the exhumation of the Alboran Sea basement and during the latest stages of its extensional history. Furthermore, at Site 976, the relative volume of the leucogranite dikes to the overall metapelite volume is too small to have acted as an additional heat source. In accordance with all of these data, there is little evidence for significant coeval magmatic activity near Site 976 or in the surrounding Alboran Domain that could have produced the considerable heating observed in the thermal evolution of the metamorphic rocks.

From the competing genetic hypotheses tested by drilling in the Alboran Sea basin (Shipboard Scientific Party, 1996a), we believe that cogent evidence from basement rocks at the Site 976 High favors models invoking wholesale removal of mantle lithosphere beneath the basin. This hypothesis appears to be clearly supported by extensive structural data from the whole region—the Betic and Rif Chains and the Alboran Basin—and is in accordance with geophysical constraints such as seismicity distribution, tomography models, gravity, and heat-flow data; even the geochemical signature of the Alboran magmatism does not contradict this proposed scenario. A northwest-dipping middle-to-latest Miocene (from 6 to at least 12 Ma; Hoernle et al., Chap. 27, this volume) oceanic-crust subduction beneath the eastern Alboran Basin, clearly confront with kinematic and structural data from the region. No evidence of coeval oceanic crust are recognized in the region, neither from geophysical nor geological data. Several geophysical data, however, might conform to a subduction model, as proposed by previous authors (see above). To verify a genetic model based solely on the nature of the magmatism, it is important to determine the areal distribution of the distinct geochemical signature in the entire volcanic region.

In conclusion, although some of the results presented here may be controversial, it is worth noting that hereafter any reliable genetic model for the origin of the Alboran Basin should be contrasted with the thermal data characterizing the metamorphic basement at Site 976. In this regard, we believe that further geological and geophysical data of the westernmost Mediterranean region are needed to validate the Leg 161 insights presented in this synthesis. to complete a definitive, fully satisfying model for the Neogene evolution of the lithosphere beneath the Alboran Sea.

SUMMARY

Ocean Drilling Program Leg 161 drilled four sites (976 to 979) in the Alboran Sea to investigate the formation and tectonic behavior of the Alboran Basin. The highest tectonic priority of Leg 161 was to sample a basement high in the West Alboran Basin at Site 976. Drilling at Sites 977, 978, and 979 was aimed at constraining the timing of the postrift deformation of the basin. The integration of drilling results with regional geological and geophysical data and the interpretations of deep and shallow seismic-reflection profiles aid in constraining the structure of the crust beneath the Alboran Sea and the origin and tectonic history of the basin.

The principal conclusions of this synthesis paper are summarized as follows:

1. Site 976 was drilled on a basement high and was cored 343.19 m of high-grade metamorphic rocks in two holes. Sample results demonstrate that the Alboran Sea basin is underlain by rocks of continental origin formed of high-grade schist, gneiss, migmatitic gneiss, marble, calc-silicate rock, and granite from the Alpujarride Complex of the Alboran Crustal Domain.

2. The metamorphic basement at Site 976 has undergone high-temperature metamorphism and melting during exhumation. P-T data show high and increasing temperature in the high-grade schist (from about 550°–600°C at 10.5–8 kbar to 650–700°C at 3–4 kbar), fast exhumation (rate of 4.5 km/m.y. in the interval 20.5–18 Ma) during crustal and lithospheric stretching, and rapid cooling (from 450°C to 60°C between 20.5–18 Ma).

3. MCS profiles combined with drilling results indicate that rifting structures—major intracrustal extensional detachments—accounted for the crustal thinning beneath the basin. Effective constraints for the extension-related exhumation history at Site 976 are given by the cooling history of the basement. Thermal modeling of the P-T path indicates that the exhumation (from a burial depth of around 40 km) and extensional denuding of the Alboran Crustal Domain started during the late Oligocene (at about 27 Ma), somewhat before the marine transgression that created the Alboran Sea took place. Drilling data demonstrated that the Site 976 High was exposed to the seafloor by the late Serravallian, but near-site MCS profiles suggest that the basement high has been a submarine, or occasionally emergent relief since the early Miocene.

4. Site 976 reveals two periods of subsidence, in at 11–10.7 Ma (rate of 3 km/m.y.) and at 2.5–0 M (a rate of 0.5 km /m.y), and uplift

at 5–2.5 Ma in the West Alboran Basin. Subsidence analyses across the Alboran Basin (data from commercial wells) indicate a conspicuous lateral variation in rift-related subsidence phases, suggesting migration of the locus of extension, and probably also changes in the direction of extension during the Miocene rifting. The almost generalized gentle phase of post-Messinian subsidence, contemporaneous with the contractive reorganization of the basin and the general uplift at the basin margins, could be interpreted as thermal subsidence.

5. Sites 977 and 978 were drilled in the East Alboran Basin and sampled 598.5 m and 485 m, respectively, of equivalent sedimentary sequences ranging in age from latest Miocene?-early Pliocene to Holocene. A gravel interval containing pebbles of volcanic, metamorphic, and sedimentary rocks, sampled at both Sites 977 and 978, is associated with the base of the Pliocene–Pleistocene sequence in the Alboran Basin (the M-reflector)

6. Drilling results and seismic images in the East and South Alboran Basins (Sites 977, 978, and 979) constrain the timing and mode of the contractive reorganization of the basin. The post-Messinian to Holocene deformation mostly resulted in wrench-tectonics giving way to both transtensive (generating new depocenters; e.g. the Yusuf Basin) and transpressive conditions (producing local uplift and positive flower-structures; e.g., the Alboran Ridge), that involve the present structural organization of the basin. The post-Messinian reorganization is consistent with the north-northwest/north present-day convergence of Iberia and Africa.

7. The volcanic pebbles sampled at Sites 977 and 978 constrain several periods of middle-to-late Miocene volcanic activity in the eastern Alboran Domain that occurred at about 12 Ma, 9 Ma, and 6 Ma. Incompatible/immobile trace- element systematics in the tholeiitic to calc-alkaline rocks indicate magmatic sources containing both depleted (MORB-type) component and an ocean-island or plume-type component ("arc signature"). On the basis of their geochemical signature, an alternative model envisaging oceanic-crust subduction beneath the eastern Alboran from 6 to at least 12 Ma has been suggested. However, the geochemistry of the magmatism does not solely provide a forceful constraint to discriminate among genetic models, as similar magmatic signatures can support different geodynamic models.

8. The age, rate, and thermal behavior of extension determined at basement Site 976 provide constraints on the initial thermal structure, the exhumation, denudation history, and the processes that have modified the crust beneath the Alboran Sea since the initiation of extension. These results support mechanic models that invoke the removal of the continental lithosphere mantle for the origin of the Alboran Basin.

CLOSING REMARKS

Despite significant progress based on ODP cores obtained during Leg 161 in the Alboran Sea basin, all the tectonic aspects we contemplate in this synthesis paper deserve more extensive investigation by drilling. Deep drilling in the westernmost Mediterranean is undoubtedly the only means of addressing and solving the striking problems raised after the Leg 161 investigations. It seems clear that more detailed structural and geophysical studies of the whole region are needed; undoubtedly, further sampling of the sedimentary cover and acoustic basement in the marine basin is critical. If deeper and safe drilling is feasible in the new perspective of future ODP drilling in the next century (according to the Long Range Plan document), deep drilling (more than 2 km deep) in the West Alboran Basin will provide the unique opportunity to establish a reliable stratigraphy of sediments filling the basin in order to constrain a complete subsidence history of the extended continental crust and to allow for accurate seismic-stratigraphy correlations. Furthermore, concrete lost targets in the East Alboran Basin during Leg 161 because of our inability to go deeper than the base of the Pliocene–Pleistocene sequence at both Sites 977 and 978, as a result of technical drilling problems, merits a further attempt, as we unfortunately missed crucial information on the nature and age of synrift sediments in a key region. We are sure that a transect of deep drill sites to sample the volcanic rocks of the extremely thinned crust in the East Alboran Basin, or even the suspected oceanic crust in the South-Balearic Basin, will probably open innovative perspectives for further investigation. Coordinated studies on the nature of the crust, distribution, and variation of magmatism signatures, and timing of tectonic and thermal subsidence history from the continental to the oceanic crust, should provide clues to the full understanding of lithosphere behavior in driving the evolution of these westernmost Mediterranean basins.

ACKNOWLEDGMENTS

We thank the Ocean Drilling Program for providing us with the unique opportunity for spectacularly achieving the tectonic objectives in the Alboran Basin. We are grateful for the help at sea of the ODP technical staff and the entire SEDCO-FOREX crew of Leg 161. We appreciate constructive comments and revisions done by B. Taylor, A. Klaus, and an anonymous reviewer that helped to improve the final version of the paper. We also acknowledge the data, preprints, and encouraging discussions of our shipboard and shorebased colleagues who participated in Leg 161's result papers. Research by M.C. Comas and J.I. Soto was supported by Project AMB95-1557 (CICYT, Spain). Research by J.P. Platt was supported by grant number GR3/10828 from the Natural Environmental Research Council of Great Britain.

REFERENCES

Aït Brahim, L., and Chotin, P., 1989. Genése et deformation des bassins néogènes du Rif Central (Maroc) au cours du rapprochement Europa-Africa. *Geodin. Acta* (Paris), 3:295–304.

Aldaya, F., Alvarez, F., Galindo-Zaldívar, J., González-Lodeiro, F., Jabaloy, A., and Navarro-Vila, F., 1991. The Malaguide-Alpujárride contact (Betic Cordillera, Spain): a brittle extensional detachment. *C. R. Acad. Sci. Paris*, 313:1447–1453.

Andriessen, P.A.M., and Zeck, H.P., 1996. Fission-track constraints on timing of Alpine nappe emplacement and rates of cooling and exhumation, Torrox area, Betic Cordilleras, S. Spain. *Chem. Geol.*, 131:199–206.

Aparicio, A., Mitjavila, J.M., Araña, V., and Villa, I.M., 1991. La edad del volcanismo de las islas Columbrete Grande y Alborán (Mediterráneo occidental). *Bol. Geol. Min.*, 102:562–570.

Araña, V., and Vegas, R., 1974. Plate tectonics and volcanism in the Gibraltar Arc. *Tectonophysics*, 24:197–212.

Azañón, J.M., Crespo-Blanc, A., and García-Dueñas, V., 1997. Continental collision, crustal thinning and nappe forming during the pre-Miocene evolution of the Alpujarride Complex (Alboran Domain, Betics), 1997. *J. Struct. Geol.*, 19:1055–1071.

Azañón, J.M., García-Dueñas, V., and Goffé, B., 1998. Exhumation of high-pressure metapelites and coeval extension in the Alpujárride (Cordilleras Bético-Rifeñas). *Tectonophysics*, 285:231–251.

Bakker, H.E., De Jong, K., Helmers, H., and Biermann, C., 1989. The geodynamic evolution of the internal zone of the Betic Cordilleras (south-east Spain): a model based on structural analysis and geothermobarometry. *J. Metamorph. Geol.*, 7:359–381.

Balanyá, J.C., and García-Dueñas, V., 1987. Les directions structurales dans le Domaine d'Alboran de part et d'autre du Détroit de Gibraltar. *C. R. Acad. Sci. Ser. 2*, 304:929–932.

————, 1988. El cabalgamiento cortical de Gibraltar y la tectónica de Béticas y Rif. *2nd Congr. Geol. España (Simposios)*, 35–44.

Balanyá, J.C., García-Dueñas, V., Azañón, J.M., and Sánchez-Gómez, M., 1997. Alternating contractional and extensional events in he Alpujarride nappes of the Alboran Domain (Betics, Gibraltar Arc). *Tectonics*, 16:189–204.

Banda, E., and Ansorge, J., 1980. Crustal structure under the central and eastern part of the Betic Cordillera. *Geophys. J. R. Astron. Soc.*, 63:515–532.

Banda, E., Gallart, J., García-Dueñas, V., Danobeitia, J., and Makris, J., 1993. Lateral variation of the crust in the Iberia Peninsula: new evidence for the Betic Cordillera. *Tectonophysics*, 221:53–66.

Banks, C.J., and Warburton, J., 1991. Mid-crustal detachment in the Betic system of southern Spain. *Tectonophysics*, 191:275–289.

Bellon, H., Bordet, P., and Montenat, C., 1983. Le magmatisme néogène des Cordillères bétiques (Espagne): cronologie et principaux caractères géochimiques. *Bull. Soc. Geol. Fr.*, Ser. 7, 25:205–218.

Berman, R.G., 1988. Internally-consistent thermodynamic data for minerals in the system Na_2O-K_2O-CaO-MgO-FeO-Fe_2O_3-Al_2O_3-SiO_2-TiO_2-H_2O-CO_2. *J. Petrol.*, 292:445–522.

Bird, P., 1978. Initiation of intracontinental subduction in the Himalaya. *J. Geophys. Res.*, 83:4975–4987.

Blanco, M.J., and Spakman, W., 1993. The P-wave velocity structure of the mantle below the Iberian Peninsula: evidence for subducted lithosphere below southern Spain. *Tectonophysics*, 221:13–34.

Bonini, W.E., Loomis, T.P., and Robertson J.D., 1973. Gravity anomalies, ultramafic intrusions, and the tectonic of the region around the Straits of Gibraltar. *J. Geophys. Res.*, 78:1372–1382.

Bourgois, J., Mauffret, A., Ammar, A., and Demnati, N.A., 1992. Multichannel seismic data imaging of inversion tectonics of the Alboran Ridge (Western Mediterranean Sea). *Geo-Mar. Lett.*, 12:117–122.

Buforn, E., Sanz de Galdeano, C., and Udías, A., 1995. Seismotectonics of the Ibero-Maghrebian region. *Tectonophysics*, 248:247–261.

Buforn, E., Udias, A., and Madariaga, R., 1991. Intermediate and deep earthquakes in Spain. *Pure Appl. Geophys.*, 136:375–393.

Calvet, A., Gomez, F., Seber, D., Barazangi, N.J., Ibenbrahim, A., and Demnati, A., 1997. An integrated geophysical investigation of recent seismicity in the Al-Hoceima Region of North Morocco. *Bull. Seis. Soc. Am.*, 87:637–651.

Carbonell, R., Torne, M., García-Dueñas, V., Moya, R., and Banda, E., 1997. The ESCI-Béticas: a seismic reflection image of the Betics orogen. *Rev. Soc. Geol. Esp.*, 8:503–512.

Chalouan, A., Saji, R., Michard, A., and Bally, A.W., 1997. Neogene tectonic evolution of the southwestern Alboran Basin as inferred from seismic data off Morocco. *AAPG Bull.*, 81:1161–1184.

Channell, J.E.T., and Mareschal, J.C., 1989. Delamination and asymmetric lithospheric thickening in the development of the Tyrrhenian Rift. *In* Coward, M.P., Dietrich, D., and Park, R.G. (Eds.), *Conference on Alpine Tectonics:* Geol. Soc. Spec. Publ. London, 45:285–302.

Cita, M.B., and McKenzie, J.A., 1986. The terminal Miocene event. *In* Hsü, K.J. (Ed.), *Mesozoic and Cenozoic Oceans.* AGU Geodyn. Ser., 15:123–140.

Comas, M.C., 1996. The Alboran Sea and the Betic-Rif orogen: aftermath of extension and compression in the Alboran Basin [paper presented at "The Mediterranean Basins: Tertiary Extension within the Alpine Orogen: An International Workshop," Cergy-Pontois, Paris, December 1996]. (Abstract)

Comas, M.C., Dañobeitia, J.J., Alvarez-Marrón, J., and Soto, J.I., 1997. Crustal reflections and structure in the Alboran Basin: preliminary results of the ESCI-Alboran Survey. *Rev. Soc. Geol. Esp.*, 8:76–88.

Comas, M.C., García-Dueñas, V., and Jurado, M.J., 1992. Neogene tectonic evolution of the Alboran Basin from MCS data. *Geo-Mar. Lett.*, 12:157–164.

Comas, M.C., García-Dueñas, V., Soto, J.I., and Campos, J., 1993. An extensional basin developed on a collisional orogen: the Alborán Sea. *In* Seranne, M., and Malavielle, J. (Eds.), *Late Orogenic Extension in Mountain Belts.* Doc. B.R.G.M. Fr., 219:44–46.

Comas, M.C., Zahn, R., Klaus, A., et al., 1996. *Proc. ODP, Init. Repts.*, 161: College Station, TX (Ocean Drilling Program).

Crespo-Blanc, A., Orozco, M., and García-Dueñas, V., 1994. Extension versus compression during the Miocene tectonic evolution of the Betic Chain: late folding of normal fault systems. *Tectonics*, 13:78–88.

De Jong, K., 1991. Tectono-metamorphic studies and radiometric dating in the Betic Cordilleras (SE Spain): with implications of extension and compression in the western Mediterranean area [Ph.D. thesis]. Vrije Univ., Amsterdam.

de la Linde, J., Comas, M.C., and Soto, J.I., 1996. Morfología del basamento en el nor-oeste del Mar de Alborán. *Geogaceta*, 20:355–358.

de Larouzière, F.D., 1985. Etude tectono-sédimentaire et magmatique des bassins néogènes d'Hinojar et de Mazarrón (Cordillères Bétiques Internes, Espagne) [Thesis 3e cycle]. Univ. Paris VI.

de Larouzière, F.D., Bolze, J., Bordet, P., Hernandez, J., Montenat, C., and Ott d'Estevou, P., 1988. The Betic segment of the lithospheric trans-Alboran shear zone during the Late Miocene. *Tectonophysics*, 152:41–52.

Dewey, J.F., Helman, M.L., Turco, E., Hutton, D.H.W., and Knott, S.D., 1989. Kinematics of the western Mediterranean. *In* Coward, M.P., Dietrich, D., and Park, R.G. (Eds.), *Conference on Alpine Tectonics.* Geol. Soc. Spec. Publ. London, 45:265–283.

Di Battistini, G., Toscani, L., Iaccarino, S., and Villa, I.M., 1987. K/Ar ages and the geological setting of calc-alkaline volcanic rocks from Sierra de Gata, SE Spain. *Neues Jahrb. Mineral.*, 8:369–383.

Docherty, J.I.C., and Banda, E., 1992. A note on the subsidence history of the northern margin of the Alboran Sea. *Geo-Mar. Lett.*, 12:82–87.

————, 1995. Evidence for the eastward migration of the Alboran Sea based on regional subsidence analysis: a case for basin formation by delamination of the subcrustal lithosphere? *Tectonics*, 14:804–818.

England, P.C., and Houseman, G.A., 1989. Extension during continental convergence, with application to the Tibetan plateau. *J. Geophys. Res.* 94:561–579.

Fernandez-Soler, J.M.F., 1992. El volcanismo calco-alcalino de Cabo de Gata (Almeria): estudio vulcanologico y petrografico. [Ph.D. dissert.]. Univ. de Granada.

Fernández-Soler, J.M.F., 1996. *El volcanismo calco-alcalino en el Parque Natural de Cabo de Gata-Níjar (Almeria): estudio volcanologico y petrografico*. Monogr. Medio Nat., Soc. Esp. Hist. Natural-Junta de Andalucia, Almeria.

Frizon de Lamotte, D., 1987. Un exemple de collage synmétamorphe: la déformation miocène des Temsamane (Rif externe, Maroc). *Bull. Soc. Geol. Fr.*, 3:337–344.

Galdeano, A., Courtillot, V., Le Borgne, E., Le Mouel, J.-L., and Rossignol, J.-C., 1974. An aeromagnetic survey of the southwest of the western Mediterranean: description and tectonic implications. *Earth Planet. Sci. Lett.*, 23:323–336.

Galindo-Zaldívar, J., González-Lodeiro, F., and Jabaloy, A., 1989. Progressive extensional shear structures in a detachment contact in the Western Sierra Nevada (Betic Cordilleras, Spain). *Geodin. Acta*, 3:73–85.

————, 1993. Stress and paleostress in the Betic-Rif cordilleras (Miocene to the present). *Tectonophysics*, 227:105–126.

Galindo-Zaldívar, J., Jabaloy, A., González-Lodeiro, F., and Aldaya, F., 1997. Crustal structure of the central sector of the Betic Cordillera (SE Spain). *Tectonics*, 16:18–37.

García-Casco, A., and Torres-Roldán, R.L., 1996. Disequilibrium induced by fast decompression in St-Bt-Grt-Ky-Sil-And metapelites from the Betic Belt (Southern Spain). *J. Petrol.*, 37:1207–1239.

García-Dueñas, V., Balanyá, J.C., and Martínez-Martínez, J.M., 1992. Miocene extensional detachments in the outcropping basement of the northern Alboran basin (Betics) and their tectonic implications. *Geo-Mar. Lett.*, 12:88–95.

García-Dueñas, V., Banda, E., Torné, M., Córdoba, D., and the ESCI-Béticas Working Group, 1994. A deep seismic reflection survey across the Betic Chain (southern Spain): first results. *Tectonophysics*, 232:77–89.

García-Dueñas, V., Martinez-Martinez, J.M., Orozco, M., and Soto, J.I., 1988. Plis-nappes, cisaillements syn-à post-metamorphiques et cisaillements ductiles-fragiles en distension dans les Nevado-Filábrides (Cordillères Bétiques, Espagne). *C. R. Acad. Sci. Paris*, 307:1389–1395.

Gibbs, A.D., 1984. Structural evolution of extensional basin margins. *J. Geol. Soc. London*, 141:609–620.

Gierman, G., Pfannenstiel, M., and Wimmenauer, W., 1968. Relation entre morphologie tectonique et volcanisme en mer d'Alboran (Mediterranée occidentale). *C. R. Somm. Soc. Geol. Fr.*, 4:116–118.

Goffé, B., Michard, A., García-Dueñas, V., González Lodeiro, F., Monié, P., Campos, J., Galindo-Zaldivar, J., Jabaloy, A., Martínez-Martínez, J.M., and Simancas, F., 1989. First evidence of high-pressure, low-temperature metamorphism in the Alpujarride nappes, Betic Cordilleras (S.E. Spain). *Eur. J. Mineral.*, 1:139–142.

Grimison, N.L., and Chen, W.-P., 1986. The Azores-Gibraltar plate boundary: focal mechanisms, depths of earthquakes, and their tectonic implications. *J. Geophys. Res.*, 91:2029–2047.

Hatzfeld, D., 1976. Etude sismologique et gravimétrique de la structure profonde de la mer d'Alboran: mise in evidence d'un manteau anormal. *C. R. Acad. Sci. Paris*, 283:1021–1024.

Hernández, J., and Bellon, H., 1985. Chronologie K-Ar du volcanisme miocéne. *Rev. Geol. Geogr. Phys.*, 26:85–94.

Hernandez, J., de Larouzière, F.D., Bolze, J., and Bordet, P., 1987. Le magmatisme néogène bético-rifain et le couloir de décrochement trans-Alboran. *Bull. Soc. Geol. Fr.*, 3:257–267.

Horvath, F., and Berckhemer, H., 1982. Mediterranean back arc basins. *In* Berckhemer, H., and Hsü, K.J. (Eds.), *Alpine-Mediterranean Geodynamics*. Am. Geophys. Union Geodyn. Ser., 7:141–173.

Jabaloy, A., Galindo-Zaldívar, J., and González-Lodeiro, F., 1993. The Alpujarride-Nevado-Filábride extensional shear zone, Betic Cordilleras, SE Spain. *J. Struct. Geol.*, 15:555–569.

Johannes, W., and Holtz, F., 1996. *Petrogenesis and Experimental Petrology of Granitic Rocks:* Berlin (Springer-Verlag).

Jurado, M.J., and Comas, M.C., 1992. Well log interpretation and seismic character of the Cenozoic sequence in the Northern Alboran Sea. *Geo-Mar. Lett.*, 12:129–136.

Kay, R.W., and Kay, M., 1993. Delamination and delamination magmatism. *Tectonophysics*, 219:177–189.

Keller, J.V.A., Hall, S.H., Dart, C.J., and McClay, K.R., 1995. The geometry and evolution of a transpressional strike-slip system: the Carboneras fault, SE Spain. *J. Geol. Soc. London*, 152:339–352.

Kirker, A.I., and Platt, J.P., 1998. Unidirectional slip vectors in the western Betic Cordillera: implications for the formation of the Gibraltar arc. *J. Geol. Soc. London*, 155:193–207.

Klaus, A., and Shipboard Scientific Party, 1996. Underway geophysics. *In* Comas, M.C., Zahn, R., Klaus, A., et al., *Proc. ODP, Init. Repts.*, 161: College Station, TX (Ocean Drilling Program), 51–52.

Kornprobst, J., 1973. Petrographical studies of "acoustic basement" and associated breccia at Site 121—western Alboran Basin: a comparison with the Betico-Rifean basement. *In* Ryan, W.B.F., Hsü, K.J., et al., *Init. Repts. DSDP*, 13 (Pt. 2): Washington (U.S. Govt. Printing Office), 759–761.

Lonergan, L., and Platt, J.P., 1995. The Malaguide-Alpujarride boundary: a major extensional contact in the Internal Zone of the eastern Betic Cordillera, SE Spain. *J. Struct. Geol.*, 17:1655–1671.

Lonergan, L., Platt, J.P., and Gallagher, L., 1994. The Internal/External Zone boundary in the Eastern Betic Cordillera, SE Spain. *J. Struct. Geol.*, 16:175–188.

Lonergan, L., and White N., 1997. Origin of the Betic-Rif mountain belt. *Tectonics*, 16:504–522.

Louni-Hacini, A., Bellon, H., Maury, R.C., Megartsi, M., Coulon, C., Semroud, B., Cotten, J., and Coutelle, A., 1995. Datation $^{40}K/^{40}Ar$ de la transition du volcanisme calco-alcalin au volcanisme alcalin en Oraine au Miocène supérieur. *C. R. Acad. Sci. Paris*, 321:972–982.

Lundeen, M.T., 1978. Emplacement of the Ronda peridotite, Sierra Bermeja, Spain. *Geol. Soc. Am. Bull.*, 89:172–180.

Maldonado, A., Campillo, A.C., Mauffret, A., Alonso, B., Woodside, J., and Campos, J., 1992. Alboran Sea late Cenozoic tectonic and stratigraphic evolution. *Geo-Mar. Lett.*, 12:179–186.

Martínez-Martínez, J.M., and Azañón, J.M., 1997. Mode of extensional tectonics in the southeastern betics (SE Spain): implications for the tectonic evolution of the peri-alboran orogenic system. *Tectonics*, 16:205–225.

Martínez-Martínez, J.M., Soto, J.I., and Balanyá, J.C., 1997. Large scale structures in the Nevado-Filábride Complex and crustal seismics fabrics of the deep seismic reflection profile ESCI-Béticas 2. *Bol. Soc. Geol. Esp.*, 477–489.

————, in press. Crustal decoupling and intracrustal flow beneath domal exhumed core complexes, Betics (SE Spain). *Terra Nova*.

Mauffret, A., El-Robrini, M., and Gennesseaux, M., 1987. Indice de la compression récente en mer Méditerranée: un bassin losangique sur la marge nor-algérienne. *Bull. Soc. Geol. Fr.*, 8:1195–1206.

Mauffret, A., Maldonado, A., and Campillo, A.C., 1992. Tectonic framework of the Eastern Alboran and Western Algerian Basins, Western Mediterranean. *Geo-Mar. Lett.*, 12:104–110.

Mazzoli, S., and Helman, M., 1994. Neogene patterns of relative plate motion for Africa-Europe: some implication for recent central Mediterranean tectonics. *Geol. Rundsch.*, 83:464–468.

McKenzie, D., 1978. Some remarks on the development of sedimentary basins. *Earth Planet. Sci. Lett.*, 40:25–32.

McKenzie, D.P., and Bickle, M.J., 1988. The volume and composition of melt generated by extension of the lithosphere. *J. Petrol.*, 29:625–679.

Medialdea, T., Suriñach, E., Vegas, R., Banda, E., and Ansorge, J., 1986. Crustal structure under the western end of the Betic Cordillera (Spain). *Ann. Geophys.*, 4:345–355.

Meghraoui, M., Morel, J.L., Andrieux, J., and Dahmani, M., 1996. Tectonique plio-quaternaire de la chaîne tello-rifaine et de la mer d'Alboran: une zone complexe de convergence continent-continent. *Bull. Soc. Geol. Fr.*, 167:141–157.

Mezcua, J., and Rueda, J., 1997. Seismological evidence for a delamination process in the lithosphere under the Alboran Sea. *Geophys. J. Int.*, 129:F1–F8.

Monié, P., Torres-Roldan, R.L., and Garcia-Casco, A., 1994. Cooling and exhumation of the western Betic Cordilleras, $^{40}Ar/^{40}Ar$ thermochronological constraints on a collapsed terrane. *Tectonophysics*, 238:353–379.

Montenat, C., 1990. Les bassins Néogènes du domaine bétique oriental (Espagne): tectonique et sédimentation dans un couloir de d´crochement. *Doc. Trav. IGAL, Paris*, 12–13.

Montenat, C., Ott d'Estevou, P., De Larouzière, F.D., and Bedu, P., 1992. Originalité géodynamique des bassins Néogène du domaine Bétique orientale. *IGAL, Notes Mem.*, 1–21:11–49.

Montenat, C., Ott d'Estavou, P., and Masse, P., 1987. Tectonic sedimentary character of the Betic Neogene basins evolving in a crustal transcurrent shear zone (SE Spain). *Bull. Cent. Rech. Explor.-Prod. Elf-Aquitaine*, 11:1-22.

Morales, J., Serrano, I.,Vidal, F., and Torcal, F., 1997. The depth of the earthquake activity in the Central Betics (Southern Spain). *Geophys. Res. Lett.*, 24:3289–3292.

Morel, J.L., 1989. Etats de contrainte et cinematique de la chaine rifaine (Maroc) du Tortonien a l'actuel. *Geodin. Acta*, 3:238–294.

Morel, J.L., and Meghraoui, M., 1996. Gorringe-Alboran-Tell tectonic zone: a transpression system along the Africa-Eurasia plate boundary. *Geology*, 24:755–758.

Morley, C.K., 1992. Notes on Neogene basin history of the western Alboran Sea and its implication for the tectonic evolution of the Rif-Betics orogenic belts. *J. African Earth Sci.*, 14:57–65.

Ott D'Estevou, P., and Montenat, C., 1985. Evolution structurale de la zone bétique orientale (Espagne) du Tortonian a l'Holocene. *C. R. Acad. Sci. Paris*, 300:363–368.

Peréz-Belzuz, F., Alonso, B., and Ercilla, G., 1997. History of mud diapirism and trigger mechanisms in the Western Alboran Sea. *Tectonophysics*, 282:399–422.

Platt, J.P., 1986. Dynamics of orogenic wedges and the uplift of high-pressure metamorphic rocks. *Geol. Soc. Am. Bull.*, 97:1037–1053.

Platt, J.P., Allerton, S., Kirker, A., and Platzman, E., 1995. Origin of the western Subetic arc (Southern Spain): paleomagnetic and structural evidence. *J. Struct. Geol.*, 17:765–775.

Platt, J.P., and England, P.C., 1994. Convective removal of lithosphere beneath mountain belts: thermal and mechanical consequences. *Am. J. Sci.*, 294:307–336.

Platt, J.P., Soto, J.I., Comas, M.C., and Leg 161 Shipboard Scientists, 1996. Decompression and high-temperature–low-pressure metamorphism in the exhumed floor of an extensional basin, Alboran Sea, Western Mediterranean. *Geology*, 24:447–450.

Platt, J.P., Soto J.I., Whitehouse M.J., and Hurford A.J, in press. Thermal evolution, rate of exhumation, and tectonic significance of metamorphic rocks from the floor of the Alboran extensional basin, western Mediterranean. *Tectonics*.

Platt, J.P., and Vissers, R.L.M., 1989. Extensional collapse of thickened continental lithosphere: a working hypothesis for the Alboran Sea and Gibraltar Arc. *Geology*, 17:540–543.

Platzman, E.S., 1992. Paleomagnetic rotations and the kinematics of the Gibraltar arc. *Geology*, 20:311–314.

Platzman, E.S., Platt, J.P., and Olivier, P., 1993. Paleomagnetic rotations and fault kinematics in the Rif arc of Morocco. *J. Geol. Soc. London*, 150:707–718.

Polyak, B.G., Fernàndez, M., Khutorsky, M.D., Soto, J.I., Basov, I.A., Comas, M.C., Khain, V.Y., Alonso, B., Agapova, G.V., Mazurova, I.S., Negredo, A., Tochitsky, V.O., de la Linde, J., Bogdanov, N.A., and Banda, E., 1996. Heat flow in the Alboran Sea (the Western Mediterranean). *Tectonophysics*, 263:191–218.

Rodríguez-Fernández, J., and Sanz de Galdeano, C., 1992. Onshore Neogene Stratigraphy in the North of the Alboran Sea (Betic Internal Zones): paleogeographic implications. *Geo-Mar. Lett.*, 12:123–128.

Royden, L.H., 1993. Evolution of retreating subduction boundaries formed during continental collision. *Tectonics*, 12:629–638.

Ruppel, C., Royden, L., and Hodges, K.V., 1988. Thermal modelling of extensional tectonics: application to pressure-temperature-time histories of metamorphic rocks. *Tectonics*, 7:947–957.

Ryan, W.B.F., Hsü, K.J., et al., 1973. *Init. Repts. DSDP*, 13 (Pts. 1 and 2): Washington (U.S. Govt. Printing Office).

Sánchez-Gómez, M., García-Dueñas, V., and Muñoz, M., 1995. Relations structurales entre les Péridotites de la Sierra Bermeja et les unités alpujarrides sous-jacentes (Benahavís, Ronda, Espagne). *C. R. Acad. Sci. Ser. 2*, 321:885–892.

Sanz de Galdeano, C., and Vera, J., 1992. Stratigraphic record and paleogeographical context of the Neogene basins in the Betic Cordillera Spain. *Basin Res.*, 4:21–36.

Seber, D., Barazangi, M., Ibenbrahim, A., and Demnati, A., 1996. Geophysical evidence for lithospheric delamination beneath the Alboran Sea and Rif-Betic mountains. *Nature*, 379:785–790.

Shipboard Scientific Party, 1996a. Introduction. *In* Comas, M.C., Zahn, R., Klaus, A., et al., *Proc. ODP, Init. Repts.*, 161: College Station, TX (Ocean Drilling Program), 5–19.

————, 1996b. Site 976. *In* Comas, M.C., Zahn, R., Klaus, A., et al., *Proc. ODP, Init. Repts.*, 161: College Station, TX (Ocean Drilling Program), 179–297.

————, 1996c. Site 977. *In* Comas, M.C., Zahn, R., Klaus, A., et al., *Proc. ODP, Init. Repts.*, 161: College Station, TX (Ocean Drilling Program), 299–353.

————, 1996d. Site 978. *In* Comas, M.C., Zahn, R., Klaus, A., et al., *Proc. ODP, Init. Repts.*, 161: College Station, TX (Ocean Drilling Program), 355–388.

————, 1996e. Site 979. *In* Comas, M.C., Zahn, R., Klaus, A., et al., *Proc. ODP, Init. Repts.*, 161: College Station, TX (Ocean Drilling Program), 389–426.

Sosson, M., Morillon, A.-C., Bourgois, J., Féraud, G., Poupeau, G., and Saint-Marc, P., 1998. Late exhumation stages of the Alpujárride Complex (western Betic Cordilleras, Spain): new thermochronological and structural data on Los Reales and Ojen nappes. *Tectonophysics*, 285:253–273.

Soto, J.I., Comas, M.C., and de la Linde, J., 1996. Espesor de sedimentos en la cuenca de Alborán mediante una conversión sísmica corregida. *Geogaceta*, 20:382–385.

Soto, J.I., and Platt, J.P., in press. Petrological and structural evolution of high-grade metamorphic rocks from the floor of the Alboran Sea basin, W. Mediterranean. *J. Petrol.*

Spear, F.S., and Cheney, J.T., 1989. A petrogenetic grid for pelitic schists in the system SiO_2-Al_2O_3-FeO-MgO-K_2O-H_2O. *Contrib. Mineral. Petrol.*, 101:149–164.

Srivastava, S.P., Schouten, H., Roest, W.R., Klitgord, K.D., Kovacs, L.C., Verhoef, J., and Macnab, R., 1990. Iberian plate kinematics: a jumping plate boundary between Eurasia and Africa. *Nature*, 344:756–759.

Steiger, R.H., and Frick, U., 1973. Isotopic dating of Alboran "basement." *In* Ryan, W.B.F., Hsü, K.J., et al., *Init. Repts. DSDP*, 13 (Pt. 2): Washington (U.S. Govt. Printing Office), 762.

Tandon, K., Lorenzo, J.M., and de la Linde, J., 1998. Timing of rifting in the Alboran Sea Basin-Correlation of borehole (ODP Leg 161 and Andalucia A-1) to seismic reflection data: implications for basin formation. *Mar. Geol.*, 144:275–294.

Tatsumi, Y., and Eggins, S., 1995. *Subduction Zone Magmatism:* Ann Arbor, MI (Blackwell Science).

Torné, M., and Banda, E., 1992. Crustal thinning from the Betic Cordillera to the Alboran Sea. *Geo-Mar. Lett.*, 12:76–81.

Torné, M., Banda, E., García-Dueñas, V., and Balanyá, J.C., 1992. Mantle-lithosphere bodies in the Alboran crustal domain (Ronda Peridotites, Betic-Rifean orogenic belt). *Earth Planet. Sci. Lett.*, 110:163–171.

Torres-Roldan, R.L., Poli, G., and Peccerillo, A., 1986. An early Miocene arc–tholeiitic magmatic dike event from the Alboran-Sea: evidence for precollisional subduction and back-arc crustal extension in the westernmost Mediterranean. *Geol. Rundsch.*, 75:219–234.

Tubía, J.M., and Cuevas, J., 1986. High-temperature emplacement of the Los Reales peridotite nappe (Betic Cordillera, Spain). *J. Struct. Geol.*, 8:473–482.

Tubía, J.M., Cuevas, J., and Gil Ibarguchi, J.I., 1997. Sequential development of the metamorphic aureole beneath the Ronda peridotites and its bearing on the tectonic evolution of the Betic Cordillera. *Tectonophysics*, 279:227–252.

Tubía, J.M., and Gil-Ibarguchi, J.I., 1991. Eclogites of the Ojen nappe: a record of subduction in the Alpujárride complex (Betic Cordilleras, southern Spain). *J. Geol. Soc. London*, 148:801–804.

Vielzeuf, D., and Clemens, J.D., 1992. The fluid-absent melting of phlogopite + quartz: experiments and models. *Am. Mineral.*, 77:1206–1222.

Watts, A.B., Platt, J.P., and Buhl, P., 1993. Tectonic evolution of the Alboran Sea Basin. *Basin Res.*, 5:153–177.

Weijermars, R., 1985. Uplift and subsidence history of the Alboran Basin and a profile of the Alboran Diapir (W-Mediterranean). *Geol. Mijnbouw*, 64:349–356.

————, 1987. The Palomares brittle-ductile shear of Southern Spain. *J. Struct. Geol.*, 9:139–157.

Westerhof, A.B., 1977. On the contact relations of high-temperature peridotites in the Serrania de Ronda, southern Spain. *Tectonophysics*, 39:579–591.

Woodside, J.M., and Maldonado, A., 1992. Styles of compressional neotectonics in the Eastern Alboran Sea. *Geo-Mar. Lett.*, 12:111–116.

Zeck, H.P., 1996. Betic-Rif orogeny: subduction of Mesozoic Tethys lithosphere under eastward drifting Iberia, slab detachment shortly before 22 Ma, and subsequent uplift and extensional tectonics. *Tectonophysics*, 254:1–16.

Zeck, H.P., Albat, F., Hansen, B.T., Torres Roldan, R.L., Garcia Casco, A., and Martin Algarra, A., 1989. A 21±2 Ma age for the termination of the ductile Alpine deformation in the internal zone of the Betic Cordilleras, south Spain. *Tectonophysics*, 169:215–220.

Zeck, H.P., Monié, P., Villa, I.M., and Hansen, B.T., 1992. Very high rates of cooling and uplift in the Alpine belt of the Betic Cordilleras, southern Spain. *Geology*, 20:79–82.

Date of initial receipt: 26 February 1998
Date of acceptance: 25 May 1998
Ms 161SR-262